LAL 09-121
LC-PHSM-2009-XXX

HZ Recoil Mass and Cross Section Analysis in ILD

K. Ito[1], H. Li[2], R. Pöschl[2], F. Richard[2],
M. Ruan[2,3], Y. Takubo[1], H. Yamamoto[1]
and the ILD Design Study Group

1- Tohoku University, Department of Physics; Aoba District, Sendai, Miyagi 980-8578, Japan

2- Laboratoire de l'Accélérateur Linéaire (LAL) -CNRS/IN2P3; B.P. 34, 91898 Orsay, France

3- Laboratoire Leprince-Ringuet (LLR), École Polytechnique - CNRS/IN2P3
Route de Saclay, 91128 Palaiseau Cedex, France

September 28, 2009

Abstract

This note describes the details of a simulation study of the Higgs boson production for processes in which the Higgs is produced together with a well measurable di-lepton system using the current proposal of the ILD detector. The analysis is optimised for the measurement of the Higgs-strahlung process, i.e. $e^+e^- \to HZ$. The cross section can be determined with a precision of 2-3% and by combining the decay channels a precision of $\sim$30 MeV is obtained for the mass of the Higgs boson. The background can be largely reduced and the analysis exhibits a sensitivity to the configuration of the accelerator.

1 Introduction

The understanding of electro-weak symmetry breaking is intimately coupled to the study of the Higgs boson. It arises as a consequence of the observation of massive gauge bosons which can be generated by the spontaneous breaking of the SU(2) × U(1) symmetry of the electroweak Lagrangian.

If existing, a Higgs boson with a mass M_H of 120 GeV as favoured by recent analyses of electro-weak data [1] will be discovered at the LHC or even at the TEVATRON. The ILC will allow for the detailed investigation of the nature of the Higgs boson as has been demonstrated in [2, 3, 4] and references therein. The relevant processes for the present study are the recoil reaction $e^+e^- \to HZ \to Hf\bar{f}$ (where f=leptons and quarks), also called *Higgs-strahlung*, or $e^+e^- \to He^+e^-$, also called ZZ fusion. The Feynman diagrams are shown in Figure 1. Please note that the cross section of the Higgs-strahlung dominates largely over that of the ZZ fusion. Hence, the analysis will be optimised for the measurement of the Higgs-strahlung process.

By detecting the decay products of the Z boson, the introduced processes and in particular the Higgs-strahlung process allow for the search of Higgs signals without any further assumption on its decay modes. In contrast to the LHC, the initial state is very well known at the ILC. These two items together allow for an unbiased search for the Higgs boson also called *Model Independent Analysis* which is only possible at a Lepton Collider such as the ILC. The presumably cleanest way to study the Higgs is given by the process $e^+e^- \to HZ$

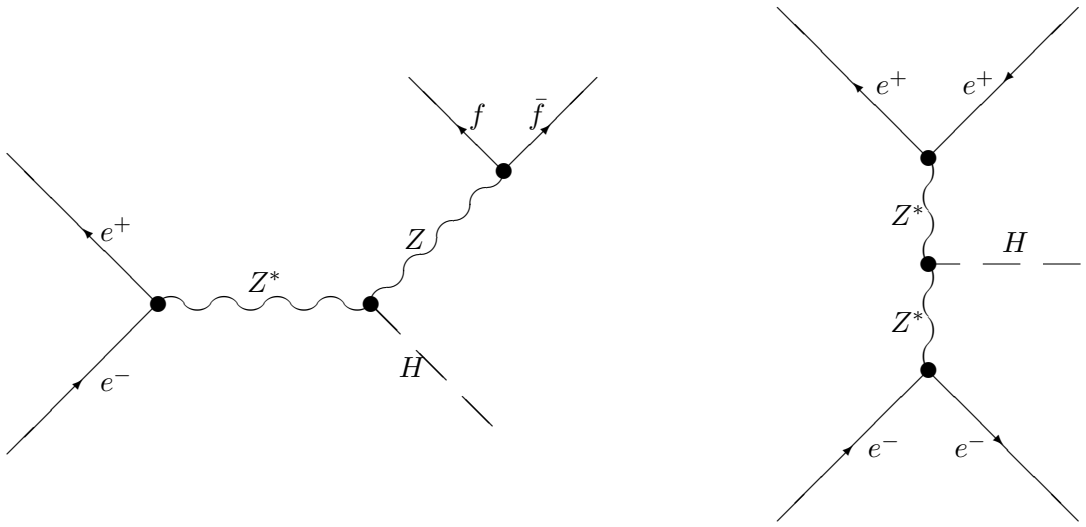

Figure 1: Higgs boson production via the Higgs-strahlung process (left) and ZZ fusion (left) and associated final state fermions with opposite charge at e^+e^--colliders.

and the subsequent decay $Z \to \mu^+\mu^-$ or $Z \to e^+e^-$, i.e. searching for the decay leptons of the well known Z boson. These channels, also named $\mu\mu X$-channel and eeX-channel hereafter, will be examined in detail in this note for a centre-of-mass energy of $\sqrt{s} = 250\,\text{GeV}$ as proposed in the definition of the benchmark scenarios for the *Letter of Intent Studies for ILC detectors* [5].

2 ILD Detector

A detailed description of the current model of the ILD detector can be found elsewhere [6]. The z-axis of the right handed co-ordinate system is given by the direction of the incoming electron beam. Polar angles given in this note are defined with respect to this axis. The most important sub-detectors for this study are described in the following.

- The vertex detector consists of three double layers of silicon extending between 16 mm and 60 mm in radius and between 62.5 mm and 125 mm in z direction. It is designed for an impact parameter resolution of $\sigma_{r\phi} = \sigma_{rz} = 5 \oplus 10/(p\sin^{\frac{3}{2}}\theta)\,\mu\text{m}$.

- The measurement of charged tracks is supported by an inner Silicon Tracker (SIT) in the central region and by a set of silicon disks in forward direction, i.e. towards large absolute values of $cos\theta$.

- The ILD detector contains a large Time Projection Chamber (TPC) with an inner sensitive radius of 395 mm and an outer sensitive radius of 1743 mm. The half length in z is 2250 mm. Recent simulation studies confirm that the momentum of charged particle tracks can be measured to a precision of $\delta(1/P_T) \sim 2 \times 10^{-5}\,\text{GeV}^{-1}$. Here P_T denotes the transverse component of the three momentum P of the particles.

- The electromagnetic calorimeter is a SiW sampling calorimeter. Its longitudinal depths of $24\,X_0$ allows for the complete absorption of photons with energies of up to 50 GeV

as relevant for the studies here. The simulated energy resolution of the electromagnetic calorimeter is $\frac{\Delta E}{E} = 15\%/\sqrt{E\,[\mathrm{GeV}]}$

- The hadronic calorimeter surrounds the electromagnetic calorimeter and comprises 4.5 interaction length λ_I. Two proposals exist for the hadronic calorimeter. A digital variant consisting of steel absorbers and gas RPC chambers with a pixel size of $1 \times 1\,\mathrm{cm}^2$ as active material. The second one features scintillating tiles with size of $3 \times 3\,\mathrm{cm}^2$ as active material. The latter option is employed in the present work.

In the current design of the ILC the initial beams enter with a crossing angle of 14 mrad. This crossing angle is not taken into account in the present study.

3 Event Generation, Detector Simulation and Event Reconstruction

All data analysed for this note have been centrally produced by the ILD Group in autumn/winter 2008/09 based on generator files known as *SLAC samples*. For the event generation the version 1.40 of the event generator WHIZARD [7] has been used. The incoming beams have been simulated with the GUINEA-PIG package [8]. The energy of the incoming beams is smeared with an energy spread of 0.28% for the electron beam and with 0.18% for the positron beam. In addition the energy is modulated by beamstrahlung. The impact on the precision of the physics result of this uncertainly will be discussed below. The generated signal and background samples are given in the Table 1 for the beam polarisation mode

$$\mathrm{e}^-_L\mathrm{e}^+_R\text{: } P_{\mathrm{e}^-} = +80\% \text{ and } P_{\mathrm{e}^+} = -30\%$$

and in Table 2 for the beam polarisation mode

$$\mathrm{e}^-_R\mathrm{e}^+_L\text{: } P_{\mathrm{e}^-} = -80\% \text{ and } P_{\mathrm{e}^+} = +30\%.$$

The initially generated samples of the signal are combined such that they yield $\mathcal{L} = 10\,\mathrm{ab}^{-1}$ in each of the polarisation modes. For background samples the integrated luminosity is mostly larger than $250\,\mathrm{fb}^{-1}$. Where it is smaller, it is still provided that the samples contain considerable statistics. Note, that in Tables 1 and 2 the background samples have been grouped by the resulting final state[1].

Due to the large cross section of the Bhabha Scattering, i.e. $\mathrm{e}^+\mathrm{e}^- \to \mathrm{e}^+\mathrm{e}^-$ and muon pair production, i.e. $\mathrm{e}^+\mathrm{e}^- \to \mu^+\mu^-$, pre-cuts have been applied in order to reduce the simulation time. These cuts are given in Table 3 and will be later on referred to as *Pre-cuts*.

Here, $M_{\mathrm{e}^+\mathrm{e}^-}$ and $M_{\mu^+\mu^-}$, respectively, are the invariant mass of the *di-lepton* system for signal events, while $P_{T\mathrm{e}^+\mathrm{e}^-}$ and $P_{T\mu^+\mu^-}$ denote the transverse momentum calculated from the vectorial sum of the two leptons.

The generated events are subject to a detailed detector simulation. The simulation is performed with the MOKKA [10] software package which provides the geometry interface to the GEANT4 [11] simulation toolkit. The event reconstruction is performed using the MarlinReco framework. For this study the versions as contained in the Software Package

[1] Please note, that due to a bug in the luminosity spectrum in the initial generation, the background has been re-weighted to the correct spectrum according to [9]

Process	Cross-Section
$\boldsymbol{\mu\mu X}$	**11.67 fb**
$\mu\mu$	10.44 pb (84.86 fb)
$\tau\tau$	6213.22 fb
$\mu\mu\nu\nu$	481.68 fb
$\mu\mu ff$	1196.79 fb

Process	Cross-Section
$\boldsymbol{eeX}$	**12.55 fb**
ee	17.30 nb (357.14 fb)
$\tau\tau$	6213.22 fb
$ee\nu\nu$	648.51 fb
$eeff$	4250.58 fb

Table 1: Processes and cross sections for polarisation mode $e^-_L e^+_R$. The signal is indicated by bold face letters; the cross-section in the parentheses of e^+e^- and $\mu^+\mu^-$ are that after Pre-Cuts, see Table 3 for the Pre-Cuts definition.

Process	Cross-Section
$\boldsymbol{\mu\mu X}$	**7.87 fb**
$\mu\mu$	8.12 pb (58.26 fb)
$\tau\tau$	4850.05 fb
$\mu\mu\nu\nu$	52.37 fb
$\mu\mu ff$	1130.01 fb

Process	Cross-Section
$\boldsymbol{eeX}$	**8.43 fb**
ee	17.30 nb (335.47 fb)
$\tau\tau$	4814.46 fb
$ee\nu\nu$	107.88 fb
$eeff$	4135.97 rb

Table 2: Processes and cross sections for polarisation mode $e^-_R e^+_L$. The signal is indicated by bold face letters; the cross-section in the parentheses of e^+e^- and $\mu^+\mu^-$ are that after Pre-Cuts, see Table 3 for the Pre-Cuts definition.

$e^+e^- \to e^+e^-$	$e^+e^- \to \mu^+\mu^-$
$\lvert cos\theta_{e^+/e^-}\rvert < 0.95$	
$M_{e^+e^-} \in (71.18, 111.18)$ GeV	$M_{\mu^+\mu^-} \in (71.18, 111.18)$ GeV
$P_{Te^+e^-} > 10$ GeV	$P_{T\mu^+\mu^-} > 10$ GeV
$M_{recoil} \in (105, 165)$ *GeV*	$M_{recoil} \in (105, 165)$ *GeV*

Table 3: List of Pre-cuts applied to Bhabha scattering and muon pair production in order to reduce the simulation time.

ILCSoft v01-06 [10] are employed. The main output of this framework for the present study are the so-called *LDC Tracks* which is a combination of track segments measured in the vertex detector, the Silicon Inner Tracker and the TPC or Forward Tracking Disks. Their momenta are compared with the energy of calorimeter clusters composed from signals in the electromagnetic and hadronic calorimeter for the particle identification.

4 Signal Selection and Background Rejection

The signal is selected by identifying two well measured leptons in the final state which yield the mass of the Z boson. The mass M_{recoil} of the system recoiling to the di-lepton system is computed using the expression:

$$M^2_{recoil} = s + M^2_Z - 2E_Z\sqrt{s}$$

Here M_Z denote the mass of the Z boson as reconstructed from the di-lepton system and E_Z its corresponding energy. A number of background processes have to be suppressed. Techniques of background suppression similar to those presented in this note were already introduced in [12]. This section firstly defines the criteria of lepton identification and then

addresses the means to suppress the background. This will be done under two assumptions: 1) model independent 2) model dependent, i.e. assuming a Higgs boson as predicted by the Standard Model. The latter excludes decay modes in which the Higgs boson decays invisibly.

4.1 Lepton Identification

The task is to identify the muons and electrons produced in the decay of the Z boson. In a first step, the energy deposition in the electromagnetic calorimeter (E_{ECAL}), the total calorimetric energy E_{total} and the measured track momentum P_{track} are compared accordingly for each final state particle. The lepton identification is mainly based on the assumption that an electron deposits all its energy in the electromagnetic calorimeter while a muon in the considered energy range, see Figure 2, passes both the electromagnetic and the hadronic calorimeter as a minimal ionising particle. The observables and cut values are summarised in Table 4.1. The motivation of the cut values can be inferred from Figure 3 where the spectra for the corresponding lepton type in the relevant momentum range $P > 15\,\mathrm{GeV}$ are compared with those from other particles are displayed.

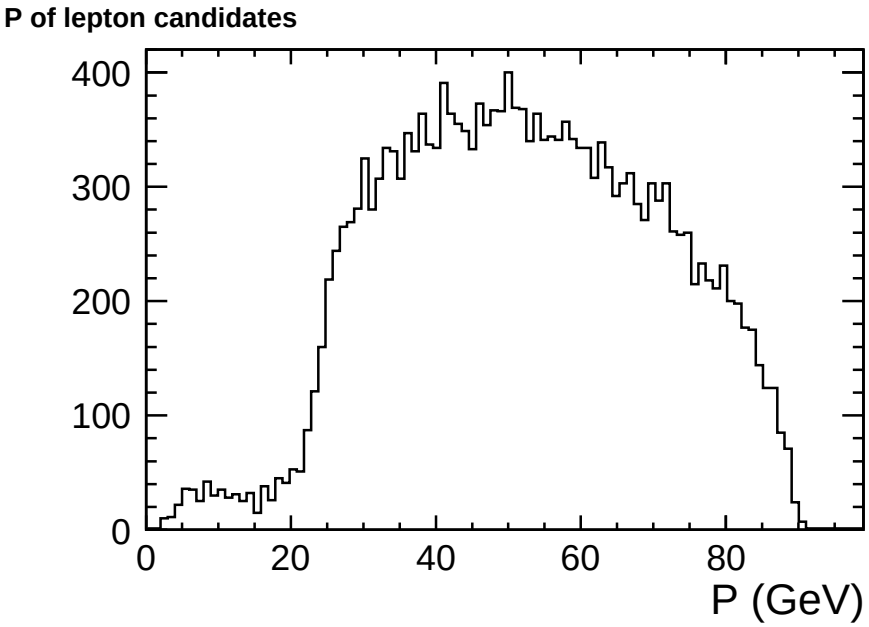

Figure 2: Momentum range of the final state leptons as produced in $\mathrm{Z} \to \mu^+\mu^-$ decays from $\mathrm{e^+e^-} \to \mathrm{HZ}$ events at $\sqrt{\mathrm{s}} = 250\,\mathrm{GeV}$.

	μ-Identification	e-Identification
E_{ECAL}/E_{total}	< 0.5	> 0.6
E_{total}/P_{track}	< 0.3	> 0.9

The criteria to estimate the quality of the lepton identification and hence the signal selection are the *Efficiency* and *Purity*. These are defined as follows:

$$\text{Efficiency} = \frac{\mathrm{N_{true \cap iden}}}{\mathrm{N_{true}}}$$

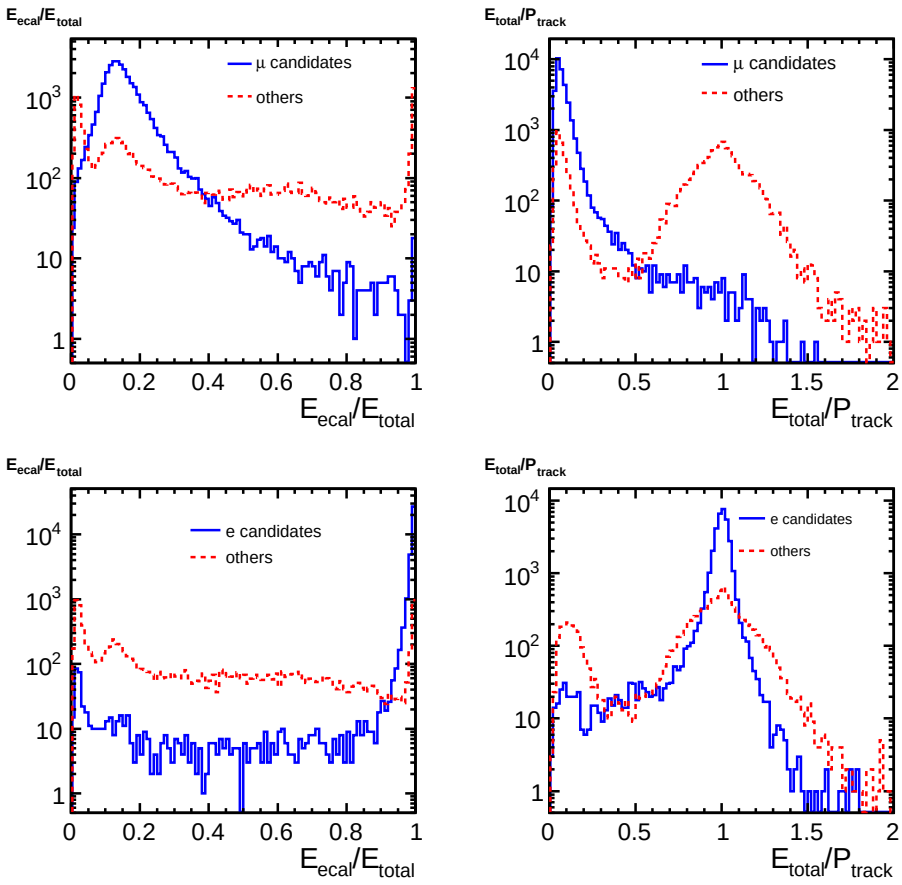

Figure 3: Distributions of the variables for lepton identification of lepton candidates and other particles with $P > 15\,\mathrm{GeV}$.

$$\text{Purity} = \frac{\mathrm{N}_{\text{true}\cap\text{iden}}}{\mathrm{N}_{\text{iden}}}$$

Here N_{true} defines the generated number of the corresponding lepton type and N_{iden} defines the reconstructed number of the corresponding lepton type according to the selection criteria. For electrons and muons with $P > 15\,\mathrm{GeV}$ in the signal samples the obtained values are listed in Table 4.

	μ *ID in* $\mu\mu X$	*e ID in* eeX
N_{true}	31833	34301
$N_{true\cap iden}$	31063	33017
N_{iden}	33986	34346
Efficiency	97.6%	96.3%
Purity	91.4%	96.1%

Table 4: Lepton ID Efficiency and Purity for reconstructed particles with $P > 15\,\mathrm{GeV}$.

The efficiencies and purities are well above 95% except for the purity of the muon identification. This is caused by final state charged pions which pass the detector as minimal ionising

particles and which are indistinguishable from muons with the applied selection criteria. This deficiency is partially balanced by the fact that two leptons of the same type with opposite charge are required for the reconstruction of the Z boson and that they should yield the mass of the Z boson. Indeed, using the above selection cuts, the efficiency to identify both leptons from the Z boson decay is 95.4% for the case $Z \to \mu\mu$ and 98.8% for the case $Z \to ee$. Note, that the cut on $P > 15\,\mathrm{GeV}$ has been omitted in this case.

4.2 Track Selection

As the invariant mass of the Z boson and thus the recoil mass will be calculated from the four momenta of the LDC Tracks, badly measured LDC Tracks need to be discarded from the analysis. The track quality can be estimated by the ratio $\Delta P/P^2$ where the uncertainty ΔP is derived from the error matrix of the given track by error propagation.

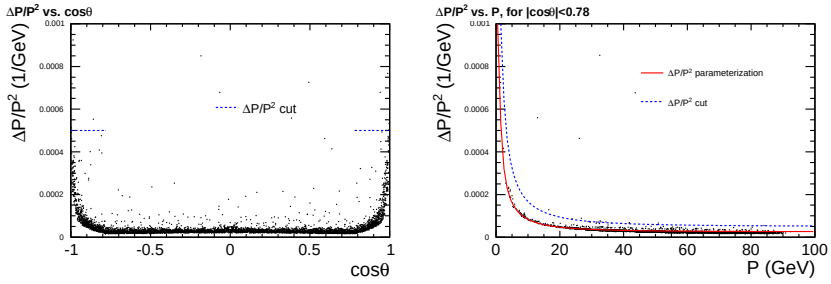

Figure 4: 2D $\Delta P/P^2$ distribution vs. $cos\theta$ (left) and $\Delta P/P^2$ distribution vs. track momentum (right) of muon candidates

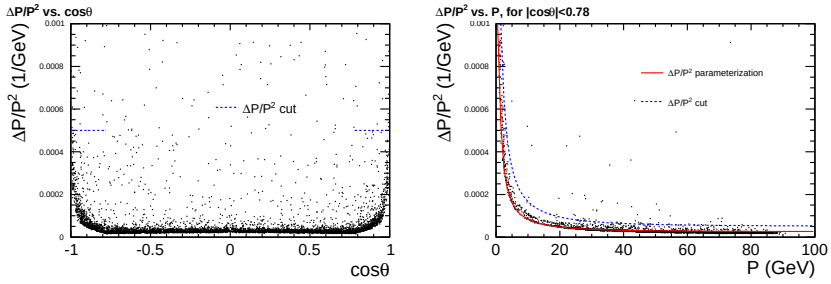

Figure 5: 2D $\Delta P/P^2$ distribution vs. $cos\theta$ (left) and $\Delta P/P^2$ distribution vs. track momentum (right) of electron candidates

The Figures 4 and 5 show, for muons and electrons separately, the dependency of $\Delta P/P^2$ on the polar angle $cos\theta$ and on the track momentum P. For reasons discussed in the following the latter has been restricted to $|cos\theta| < 0.78$, i.e. the central region. For both variables the distributions exhibit for muon tracks a narrow band with well measured momenta equivalent to small $\Delta P/P^2$. The track quality decreases as expected towards large $|cos\theta|$, i.e. towards the acceptance limits of the TPC which motivates the restriction to the central region when displaying $\Delta P/P^2$ versus P. These distributions show a decrease in track quality towards small particle momenta as expected from multiple scattering effects. Beyond that, it is clearly visible that for electrons the situation is much more diluted and the number of badly

measured tracks is significantly higher than that for muons. This can be explained by the Bremsstrahlung of the electrons in the detector material.

The procedure for track rejection is developed for the better measured muon induced tracks:

- For $|cos\theta| < 0.78$ the shape of $\Delta P/P^2$ versus P is approximated by:

$$\delta(1/P) = \Delta P/P^2 = a \oplus b/P = c(P); \text{ with } a = 2.5 \times 10^{-5}\,\text{GeV}^{-1} \text{ and } b = 8 \times 10^{-4}. \quad (1)$$

  Tracks are rejected if $\delta(1/P) > 2c(P)$.

- For $|cos\theta| > 0.78$ tracks are rejected if $\Delta P/P^2 < 5 \times 10^{-4}\,\text{GeV}^{-1}$.

The cuts are indicated in Figure 4 and 5 and underline that tracks created by electrons are rejected considerably more often which will reduce the number of reconstructed Z bosons in the corresponding channel.

4.3 Background Rejection

The recoil analysis is based on the identification of the di-lepton system as produced by the decay of the Z boson. It is thus necessary to distinguish the processes which lead to two leptons in the final state as given in Table 1 and Table 2 from the ones produced in the Higgs-strahlung process.

For the Higgs-strahlung process the invariant mass of the di-lepton system M_{dl} should be equal to the Z boson mass while the invariant mass of the recoiling system, M_{recoil} is expected to yield the introduced mass of the Higgs boson of 120 GeV. It is unlikely that combinations of background processes fulfil both conditions at once. This argumentation is supported by Figures 6 and 7 which show the invariant mass distributions for the di-lepton system and the recoil mass for both, the di-lepton system consisting of muons and the di-lepton system consisting of electrons. These distributions suggest to restrict the analysis to the following mass ranges:

- $80 < M_{dl} < 100\,\text{GeV}$
- $115 < M_{recoil} < 150\,\text{GeV}$

In a next step the selection is to be made by means of the different kinematic properties. In the following the variables used to distinguish signal events from background events will be introduced.

- Acoplanarity *acop*, see Figure 8: As for e^+e^- collisions with beams of equal energy the centre-of-mass system is at rest, it is expected that in processes in which the leptons are produced at the Z^* vertex these two leptons are back-to-back in azimuth angle. The distance in azimuth angle is expressed by the acoplanarity *acop*, defined as $acop = |\phi_{\ell^+} - \phi_{\ell^-}|$, where $\phi_{\ell^\pm}$ is the azimuth angle of the an individual lepton of the di-lepton system. If the particles are produced from a intermediate particle with a given transverse momentum, the exact back-to-back configuration is modulated. Therefore a cut on $0.2 < acop < 3$ is applied.

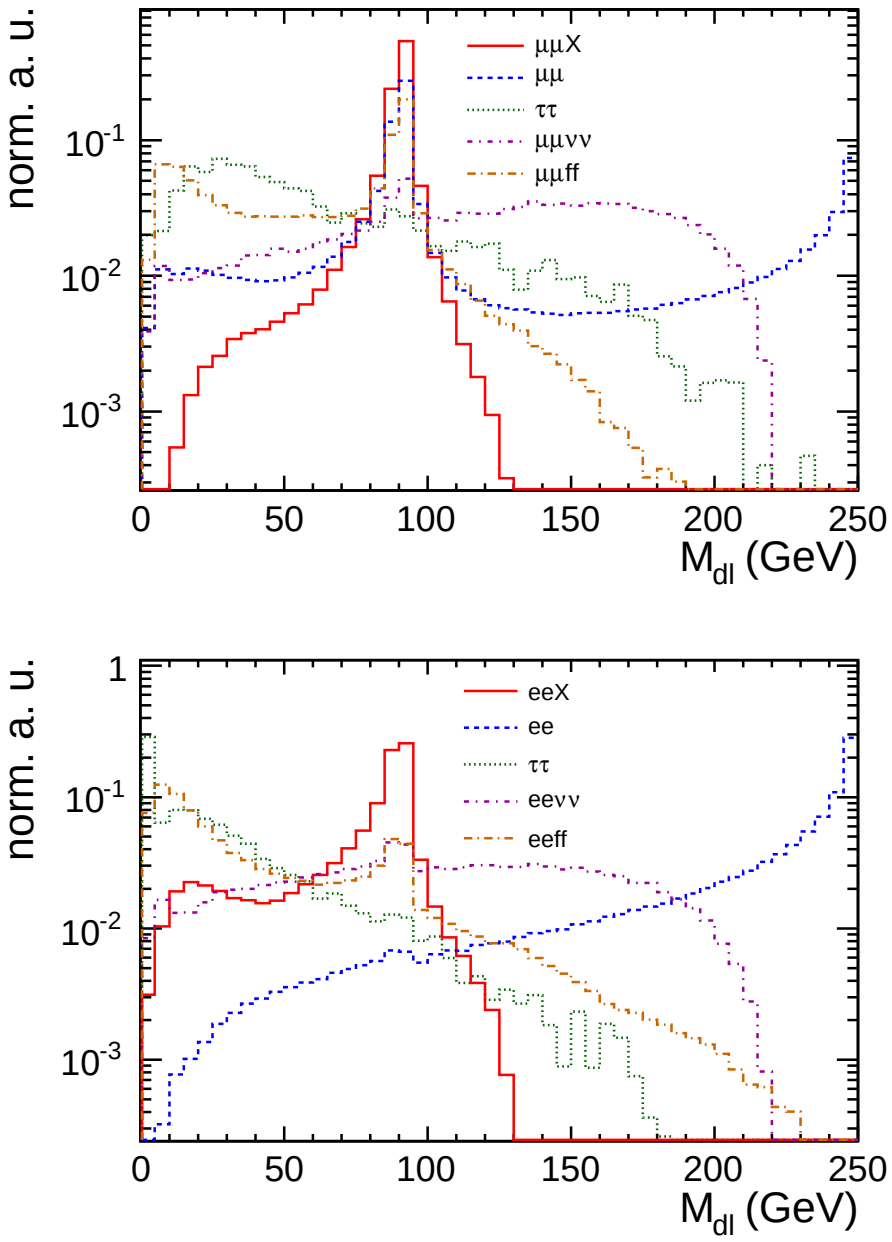

Figure 6: Normalised signal and background distributions of the invariant mass of the dilepton system M_{dl} for the $\mu^+\mu^- X$ (top) and $e^+e^- X$ Channel (bottom). Here, $\tau\tau$ refers to the $\mu\mu$ or ee created in the decay of $\tau\tau$. Note that the Pre-cuts defined in Section 3 have been applied to the $\mu\mu$ background sample.

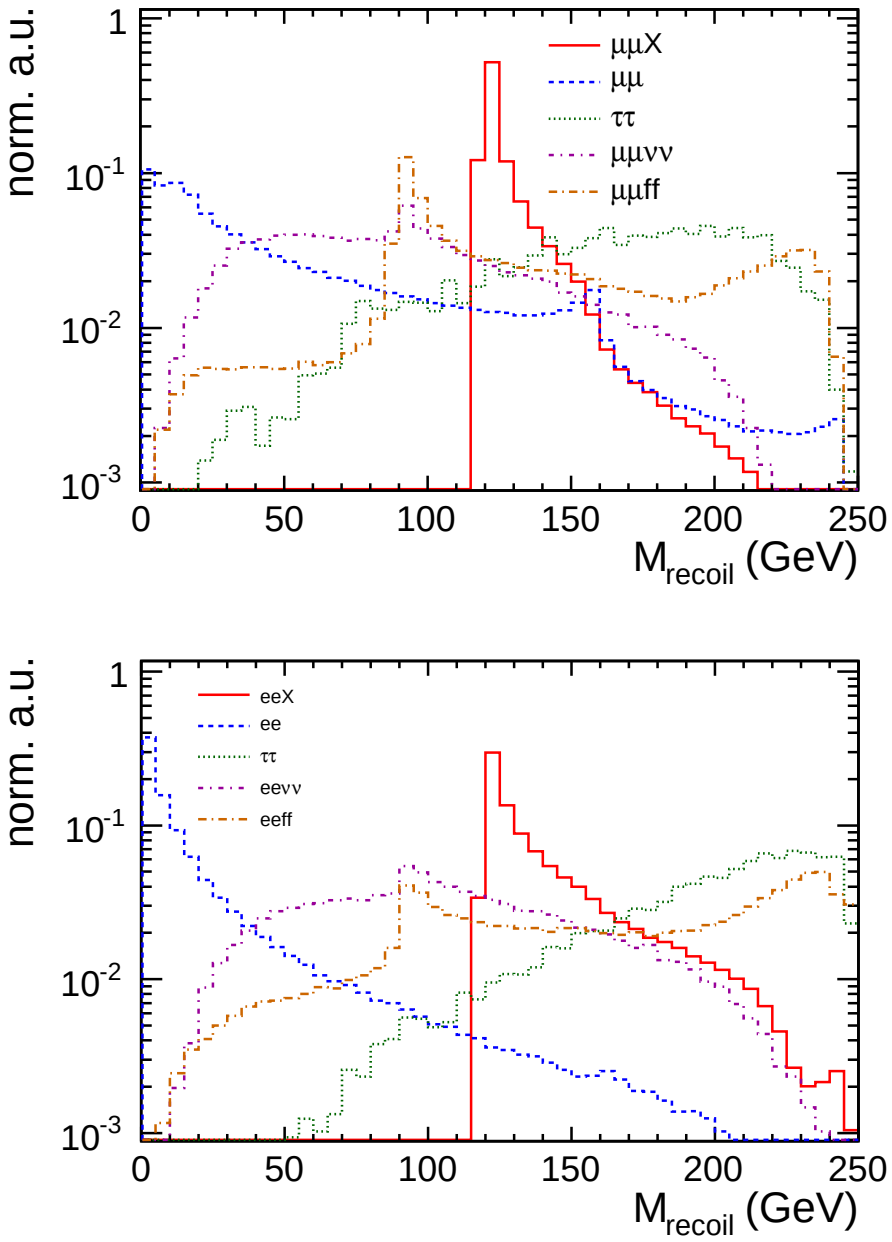

Figure 7: Normalised signal and background distributions of the recoil mass M_{recoil} distributions for the $\mu^+\mu^- X$ (top) and the $e^+e^- X$ Channel (bottom). Here, $\tau\tau$ refers to the $\mu\mu$ or ee created in the decay of $\tau\tau$. Note that the Pre-cuts defined in Section 3 have been applied to the $\mu\mu$ background sample.

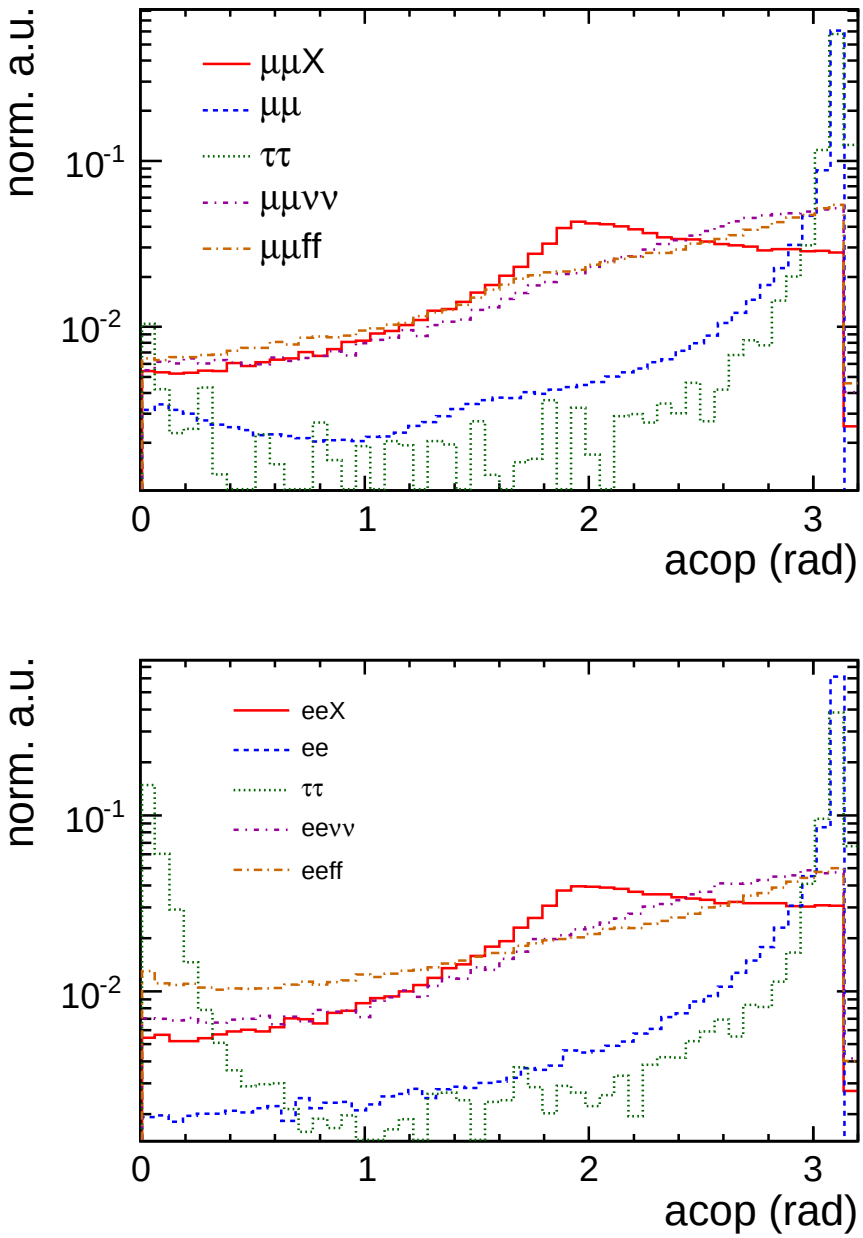

Figure 8: Normalised signal and background distributions of the acoplanarity *acop* for the $\mu^+\mu^- X$-Channel (top) and $e^+e^- X$-Channel (bottom). Here, $\tau\tau$ refers to the $\mu\mu$ or ee created in the decay of $\tau\tau$. Note that the Pre-cuts defined in Section 3 have been applied to the $\mu\mu$ background sample.

- Transverse Momentum P_{Tdl} of the di-lepton system, see Figure 9: As the Higgs-strahlung process can be interpreted as a two body decay, both bosons gain equal transverse momentum which is conserved by their decay products. The total final state for muon pair production or Bhabha Scattering has in first approximation no transverse momentum. In order to suppress this background, a cut $P_{Tdl} > 20\,\mathrm{GeV}$ of the di-lepton system is applied. This cut cannot suppress events in which initial state radiation of the incoming beams leads to a transverse momentum of the colliding system. This case will be discussed separately.

- $cos\theta_{missing}$: this cut discriminates events which are unbalanced in longitudinal momentum, essentially, those of the type $e^+e^- \to l^+l^-\gamma$. The distributions in Figure 10 motivate a cut on $|cos\theta_{missing}| < 0.99$.

The last introduced cut also suppresses events with initial state radiation happening approximately collinear with the incoming beams. The final state in $e^+e^- \to \mu^+\mu^-(e^+e^-)$ can, however, gain sizeable transverse momentum by initial state radiation of a high energetic photon. Figure 11 shows the correlation between the transverse momentum $P_{T\gamma}$ of a detected high energetic photon, assumed to be created by initial state radiation, and the transverse momentum P_{Tdl} of the di-lepton system for both, events in which only a muon pair is created at the Z^*- Boson vertex and signal events. The first type shows a clear correlation in transverse momentum. In order to suppress this background the variable $\Delta P_{Tbal.} = P_{Tdl} - P_{T\gamma}$ is introduced which is shown in Figure 12 for signal events and background events superimposed with each other. By selecting events with $\Delta P_{Tbal.} > 10\,\mathrm{GeV}$, a considerable fraction of background can be suppressed. It should finally be noted that background events of type $e^+e^- \to \mu^+\mu^-(e^+e^-)$ which are undergoing final state radiation are suppressed by the requirement that the lepton should yield the Z boson mass.

The number of events remaining after each of these cuts for signal and backgrounds are given in Tabs. 5 through 8 for two beam polarisations and the different compositions of the di-lepton system. The combination of cuts will be later referred as *MI Cuts*. Please note that the cut variables f_L and $|\Delta\theta_{2tk}|$ will be introduced later.

From the tables the following conclusions can be drawn

- The requirement to have two well measured leptons retains always more than 95% of the signal while it suppresses in most of the cases the largest part of background events.

- The requirement of a minimum P_{Tdl} of the di-lepton system is very efficient for events in which the di-lepton system is produced directly at the Z^* vertex, see Figure 1. This type of background is further reduced by comparing the transverse momentum of the di-lepton system with the transverse momentum of a radiative photon. The cut is particulary efficient to suppress background events generated by Bhabha Scattering.

- Although largely suppressed, the number of events generated by Bhabha background still exceeds the number of signal events. This remains an irreducible background.

- The acoplanarity *acop* is particularly efficient against background in which the di-lepton system is composed by τ- Leptons. The larger mass of this particle reduces the phase space for radiative processes. Hence this lepton type is more often produced in a back-to-back configuration than the lighter lepton types.

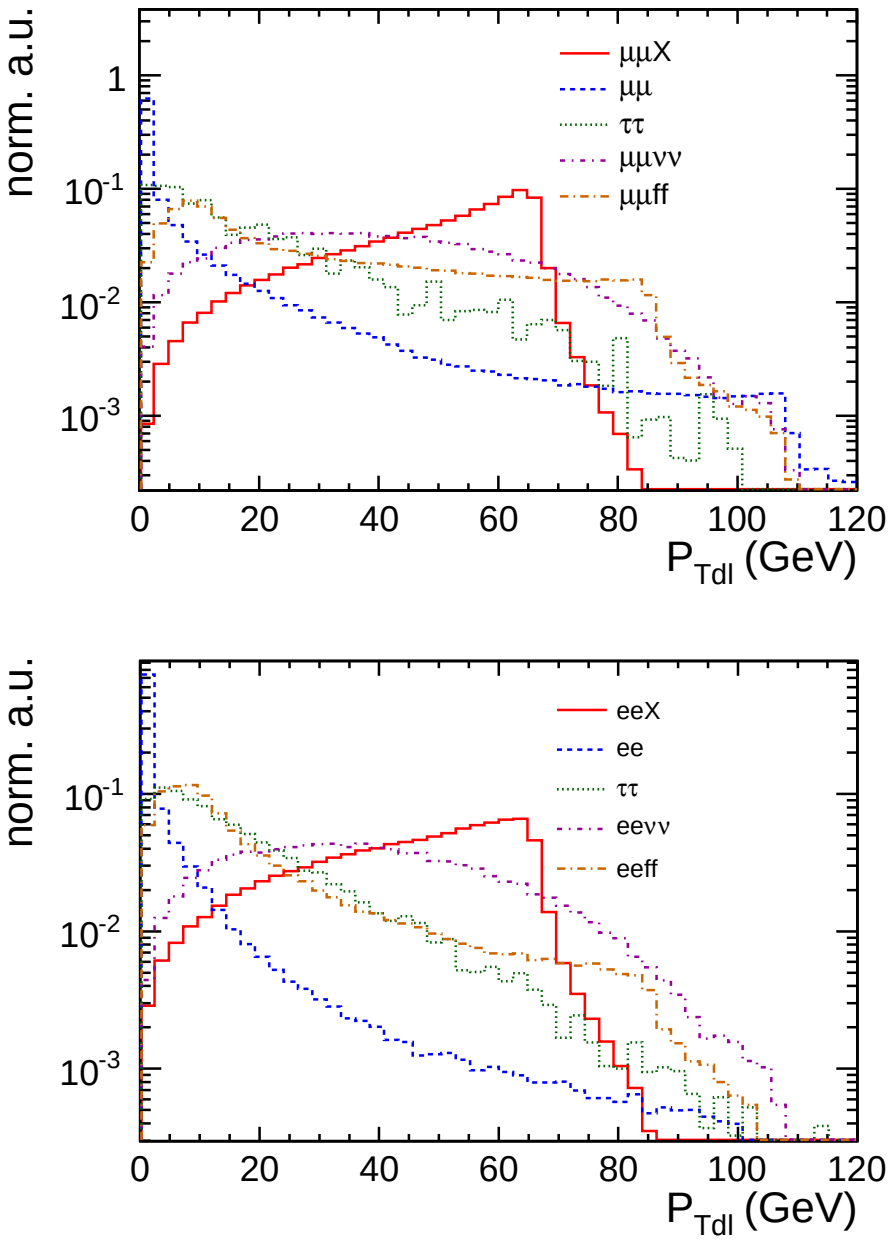

Figure 9: Normalised signal and background distribution of the transverse momentum P_{Tdl} of the dilepton system for the $\mu^+\mu^- X$ Channel (top) and the $e^+e^- X$-Channel (bottom). Here $\tau\tau$ refers to the $\mu\mu$ or ee created in the decay of $\tau\tau$. Note that the Pre-cuts defined in Section 3 have been applied to the $\mu\mu$ background sample.

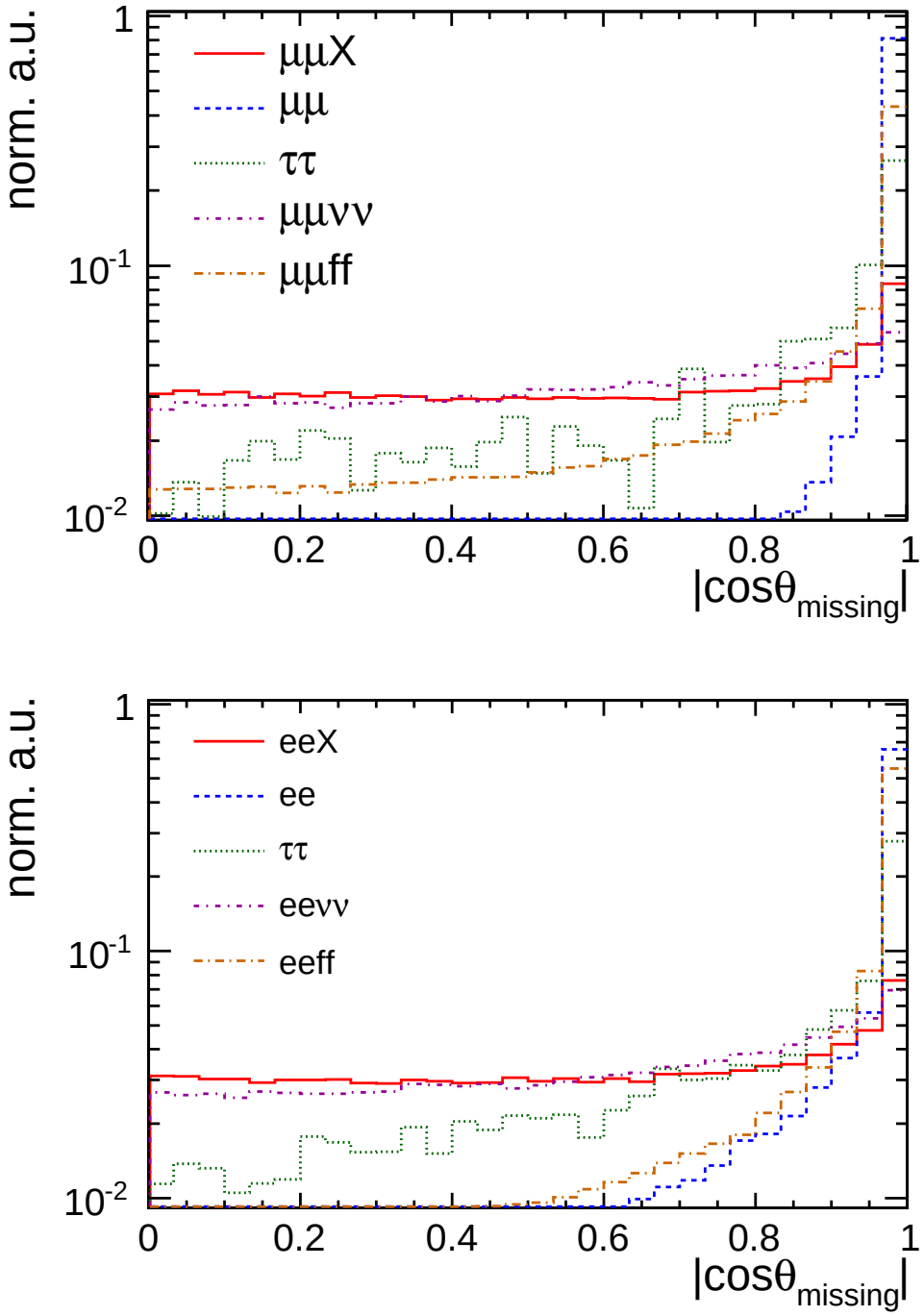

Figure 10: Normalised signal and background distributions of the $|\cos\theta_{\text{missing}}|$ of the system of undetected particles for the $\mu^+\mu^- X$-Channel (top) and $e^+e^- X$-Channel (bottom).

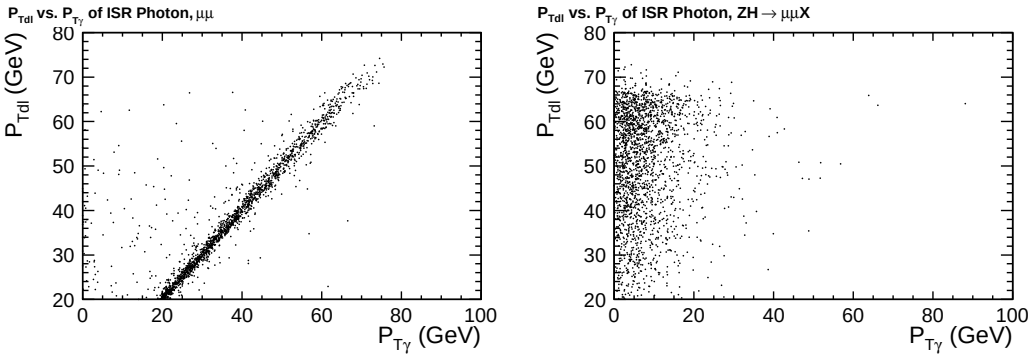

Figure 11: P_{Tdl} vs. $P_{T\gamma}$ for background by $e^+e^- \to \mu^+\mu^-$ (left) and for signal (right) in the $\mu\mu X$-channel.

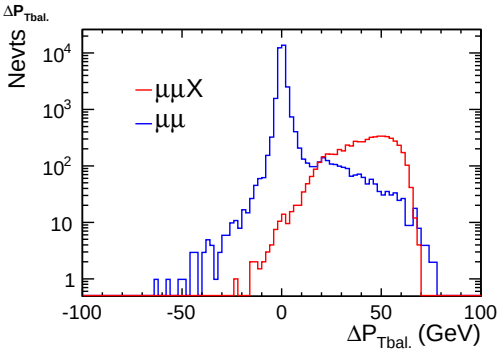

Figure 12: $\Delta P_{Tbal.}$ distributions for background by $e^+e^- \to \mu^+\mu^-$ and signal in the $\mu\mu X$-channel.

The tables demonstrate that mostly events in which the di-lepton system is produced at the Z^* vertex can be efficiently rejected by the defined cuts. The background by events in which two bosons are produced, i.e. $e^+e^- \to ZZ/\gamma\gamma$ or $e^+e^- \to W^+W^-$, is less well distinguishable from the signal events. As these events however have slightly different spectra. Further rejection can be achieved by a multi-variate analysis of a set of suited discriminative variables. These variables are introduced in the following.

- The γ-pair production leads to a flat distribution in the di-lepton mass spectrum in the Z-mass region The shape of the invariant mass M_{dl} of the di-lepton system and hence also that of the transverse momentum P_{Tdl} of the di-lepton system can be employed to suppress background from γ-pair production.

- The production of Z boson and W boson pairs happens predominantly via exchange reactions which lead to a strong increase of the differential cross section towards large absolute values of the cosine of the polar angle. On the contrary, the Higgs-strahlung process is expected to decrease towards the forward and backward direction. Therefore the polar angle spectrum as shown in Figure 13 of the di-lepton system is expected to discriminate between signal events and background from Z and W pair production.

- The acollinearity, defined as $acol = acos(\mathbf{P}_{\ell^+}\mathbf{P}_{\ell^-}/|\mathbf{P}_{\ell^+}||\mathbf{P}_{\ell^-}|)$, is sensitive to the boost of the di-lepton system. In case of Z pair production the decay products are expected

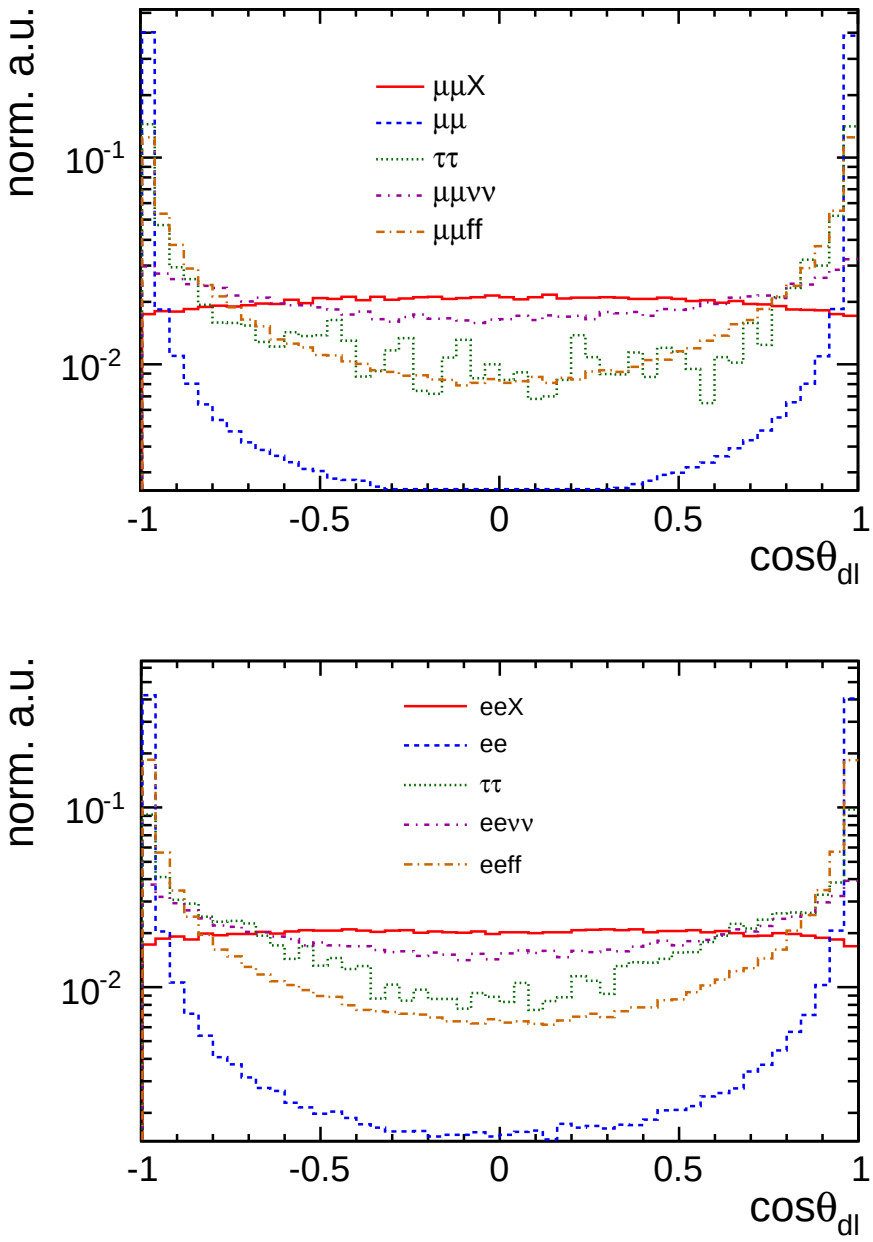

Figure 13: Normalised signal and background distribution of the cosine of the polar angle $\cos\theta_{\mathrm{dl}}$ of the di-lepton system for the $\mu^+\mu^- X$ Channel (top) and the $\mathrm{e}^+\mathrm{e}^- X$-Channel (bottom). Here $\tau\tau$ refers to the $\mu\mu$ or ee created in the decay of $\tau\tau$. Note that the Pre-cuts defined in Section 3 have been applied to the $\mu\mu$ background sample.

to be boosted more strongly than in the case of Higgs-strahlung. This results in a different position of the Jacobian Peak in the $d\sigma/d(acol)$ differential cross section as demonstrated in Figure 14.

The *likelihood* of an event to be the signal is defined as $L_S = \prod P_i^S$, where the P_i^S is the probability of the event to be the signal according to the PDF of the signal of the ith selection variable. Similarly, the likelihood of an event to be the background is defined as $L_B = \prod P_i^B$. Hereafter, the *Likelihood Fraction* is defined as $f_L = L_S/(L_S + L_B)$, which is within $(0, 1)$. The Figures 15 through 18 outline the optimisation procedure in the likelihood analysis separately for the two analysis channels and polarisation modes using the four variables introduced above, for details see [13]. It is clearly visible that the separation between signal and background improves towards small values of f_L. The cut on f_L is optmised according to the maximum in the significance $S/\sqrt{S+B}$ where S and B are the number of remaining signal and background events, respectively. The cut on f_L is adjusted for each polarisation mode of the incoming beams and the type of the di-lepton system under study.

The final number of events also included in Tables 5 through 8 shows that with the multivariate analysis the number of background events are further reduced by roughly 50% while the major part of the signal events is kept.

5 Model Dependent Analysis

If the analysis of the Higgs-strahlung process is restricted to modes in which the Higgs can solely decay into charged particles as e.g. suggested by the Standard Model, hence introducing a *Model Dependency*, the different track multiplicities can be used for the separation of signal and background events. The Higgs boson decays into oppositely charged particles such that events with less than four tracks can be considered as background. Figure 19 shows the number of reconstructed tracks beside the ones from the di-lepton system for final states of the types $\mu\mu X$, $\mu\mu$, $\tau\tau$ and $\mu\mu\nu\nu$.

As expected, the Higgs-strahlung process leads to a considerable amount of charged particles while processes with a low multiplicity of charged particles also create only a small number of tracks. The distributions tell that a large fraction of events have exactly two additional tracks beside those of the di-lepton system. The two additional tracks originate from two sources.

- Tracks created by charged particles by $\mathrm{H} \rightarrow \tau^+\tau^-$ and the subsequent decays of the τ-Leptons into charged particles.

- Tracks created by photon conversion. This photon may be created by initial state radiation.

The first type of events need to be kept in the signal as the τ-Leptons constitute an important analyser to determine e.g. quantum numbers like *CP* of the Higgs boson [2]. The second type of events can be rejected by taking into account that the opening angle of e^+e^- pair created by photon conversion is expected to be very small. This is underlined by Figure 20 which shows the angular difference $\Delta\theta_{2tk}$ between the two additional tracks. While the signal events result in a flat distribution, the background events exhibit a strong maximum around $\Delta\theta_{2tk} = 0$. This observation motivates the a cut $|\Delta\theta_{2tk}| > 0.01$. The di-lepton system of a given type might be contaminated from particles of the other type. Therefore, the polar angle of each of the two particles of the di-lepton system is also compared with the polar

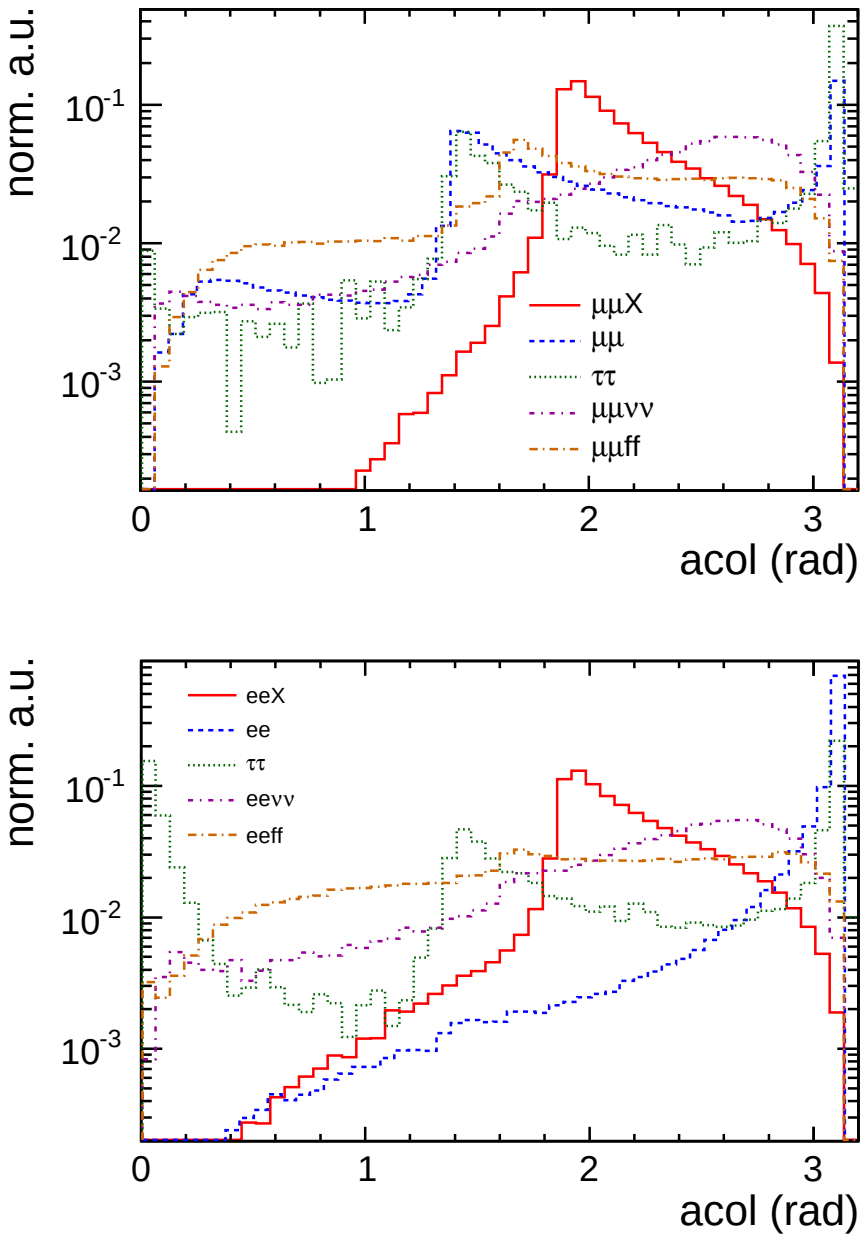

Figure 14: Normalised signal and background distribution of angle *acol* between the partners of the di-lepton system for the $\mu^+\mu^- X$ Channel (top) and the $e^+e^- X$-Channel (bottom). Here $\tau\tau$ refers to the $\mu\mu$ or ee created in the decay of $\tau\tau$. Note that the Pre-cuts defined in Section 3 have been applied to the $\mu\mu$ background sample.

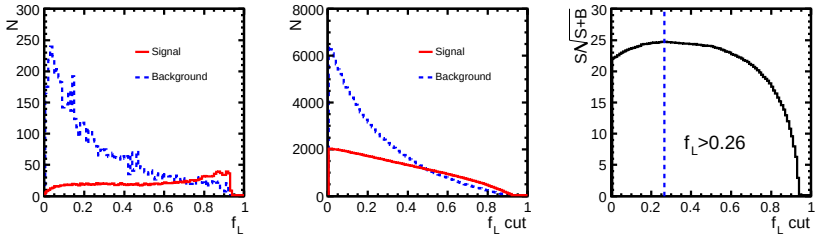

Figure 15: The distributions of the Likelihood Fraction f_L (left), the number of remaining events versus the cut on f_L (middle), and the significance versus f_L cuts (right). The distributions are shown for the $\mu\mu X$-channel in the Model Independent Analysis and for the polarisation mode $e^-_L e^+_R$.

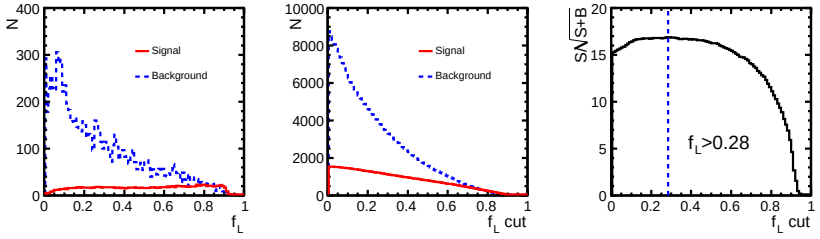

Figure 16: The distributions of the Likelihood Fraction f_L (left), the number of remaining events versus the cut on f_L (middle), and the significance versus f_L cuts (right). The distributions are shown for the eeX-channel in the Model Independent Analysis and for the polarisation mode $e^-_L e^+_R$.

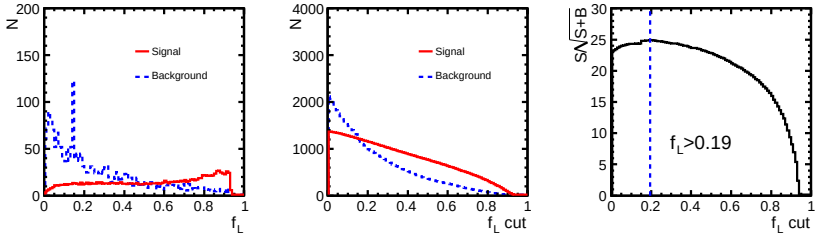

Figure 17: The distributions of the Likelihood Fraction f_L (left), the number of remaining events versus the cut on f_L (middle), and the significance versus f_L cuts (right). The distributions are shown for the $\mu\mu X$-channel in the Model Independent Analysis and for the polarisation mode $e^-_R e^+_L$.

angle of the additional tracks, defining the observable $\Delta\theta_{min}$ as shown in Figure 21. Again, a strong maximum around $\Delta\theta_{min} = 0$ can be observed which suggests the cut $\Delta\theta_{min} > 0.01$

Tables 9 through 12 give the resulting number of events after each cut applied under the assumption that the Higgs boson decays into Standard Model particles. Note, that the cut on the transverse momentum of the di-lepton system has been omitted in order to maximise the number of signal events. The combination of cuts will be later referred as *MD Cuts*. The numbers in the tables show that the cuts introduced for the additional tracks allow for an entire suppression of backgrounds with a small multiplicity of charged particles in the final

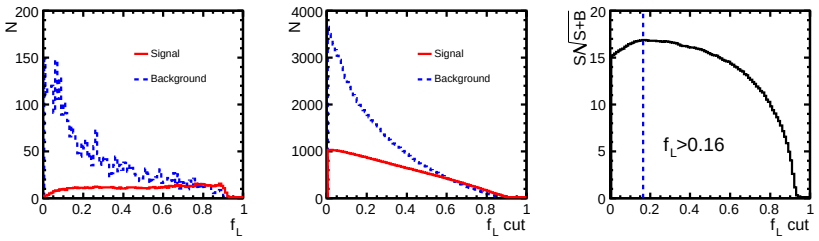

Figure 18: The distributions of the Likelihood Fraction f_L (left), the number of remaining events versus the cut on f_L (middle), and the significance versus f_L cuts (right). The distributions are shown for the eeX-channel in the Model Independent Analysis and for the polarisation mode $e^-_R e^+_L$.

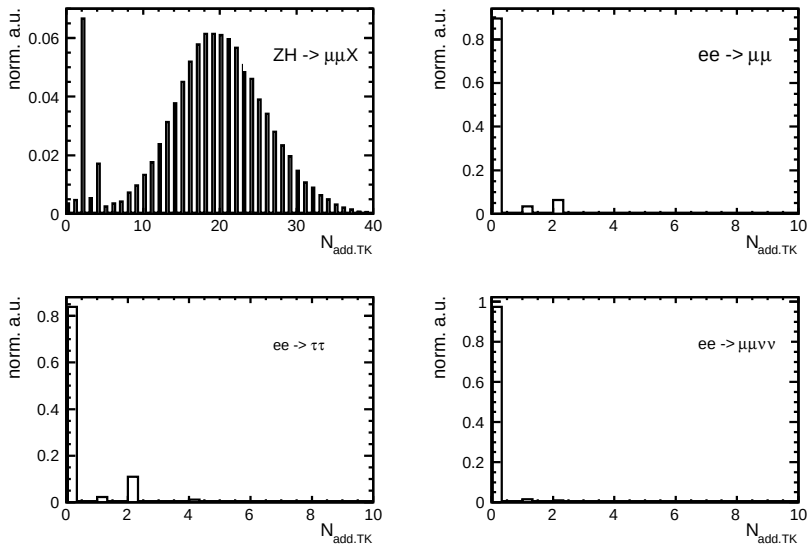

Figure 19: Number of additional tracks ($N_{add.TK}$) for $\mu\mu X$, $\mu\mu$, $\tau\tau$ and $\mu\mu\nu\nu$ final states.

state. It has to be pointed out that in particular the background from Bhabha events can be removed almost completely. On the other hand at least 50% of the signal is retained by the cuts.

Again the remaining major background is given by events in which vector bosons pairs are produced. This background is further reduced by a likelihood analysis as described above. The results of this likelihood analysis is also given in Tables 9 through 12. From these tables, it can be deferred that the f_L cuts reject the background from Z pair production by a factor of two, and reduce the signal by only 10%. At the same time, the background $\mu\mu$, ee, $\tau\tau$, $\mu\mu\nu\nu$ and $ee\nu\nu$ is entirely suppressed.

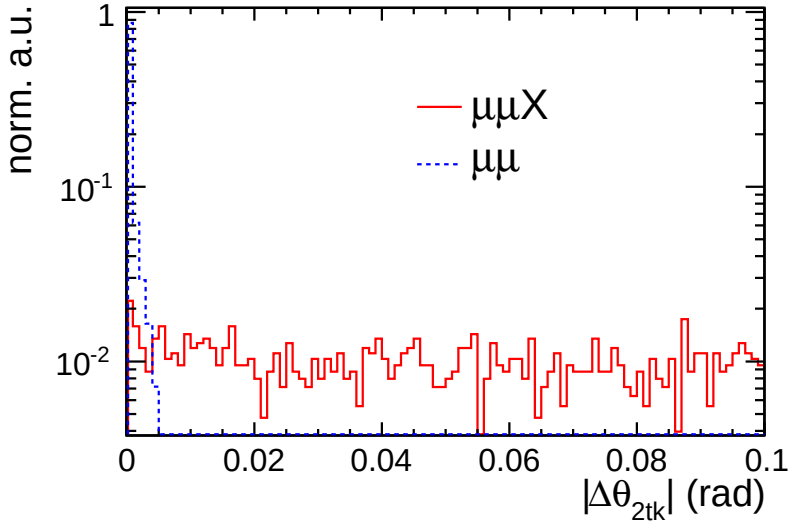

Figure 20: Distribution of $\Delta\theta_{2tk}$, which is the $\Delta\theta$ between two additional tracks for $N_{add.TK} = 2$, for signal events ($\mu\mu X$) and background by muon pair production ($\mu\mu$).

5.1 Tables of Background Rejection

MI, $\mu^+\mu^-$**X,** $e_L^-e_R^+$					
N_{evts} Remained	$\mu^+\mu^-X$	$\mu^+\mu^-$	$\tau^+\tau^-$	$\mu^+\mu^-\nu\nu$	$\mu^+\mu^-ff$
Before any restriction	2918 (100.0%)	2.6M	1.6M	111k	317k
+ Lepton ID + Tightened Pre-Cuts	2472 (84.72%)	9742	4582	9268	8175
+ $P_{Tdl} > 20$GeV	2408 (82.50%)	7862	3986	8462	7222
+ $M_{dl} \in (80, 100)$GeV	2292 (78.54%)	6299	2679	5493	5658
+ $acop \in (0.2, 3.0)$	2148 (73.61%)	5182	112	5179	5083
+ $\Delta P_{Tbal.} > 10$GeV	2107 (72.20%)	335	80	4705	4706
+ $\lvert\Delta\theta_{2tk}\rvert > 0.01$	2104 (72.11%)	149	80	4647	4676
+ $\lvert\cos\theta_{missing}\rvert < 0.99$	2046 (70.09%)	82	80	4647	3614
+ $M_{recoil} \in (115, 150)$GeV	2028 (69.48%)	75	80	3642	2640
+ $f_L > 0.26$	1596 (54.68%)	41	0	1397	1125

Table 5: Number of events remained after each cut for the $\mu^+\mu^-X$ channel in the MI Analysis. Fractions of number of events remained of the Higgs-Strahlung process are given inside parentheses, the last one gives the efficiency of signal selection. The polarisation mode is $e_L^-e_R^+$.

MI, e^+e^-**X,** $e^-_L e^+_R$					
N_{evts} Remained	e^+e^-X	e^+e^-	$\tau^+\tau^-$	$e^+e^-\nu\nu$	e^+e^-ff
Before any restriction	3138 (100.0%)	4.3G	1.6M	147k	110k
+ Lepton ID + Tightened Pre-Cuts	2019 (64.33%)	43607	6422	13196	12548
+ $P_{Tdl} > 20$GeV	1962 (62.50%)	39152	5551	12054	10583
+ $M_{dl} \in (80, 100)$GeV	1755 (55.93%)	25501	3806	7786	7509
+ $acop \in (0.2, 3.0)$	1645 (52.41%)	23228	245	7239	6739
+ $\Delta P_{Tbal.} > 10$GeV	1606 (51.16%)	1725	157	6286	5904
+ $\lvert\Delta\theta_{2tk}\rvert > 0.01$	1603 (51.09%)	990	157	6150	5844
+ $\lvert\cos\theta_{missing}\rvert < 0.99$	1564 (49.83%)	679	157	6149	4643
+ $M_{recoil} \in (115, 150)$GeV	1539 (49.04%)	576	41	4824	3335
+ $f_L > 0.28$	1153 (36.74%)	243	29	2019	1217

Table 6: Number of events left after each cut for the e^+e^-X channel in the MI Analysis. Fractions of number of events remained of the Higgs-Strahlung process are given inside parentheses, the last one gives the efficiency of signal selection. The polarisation mode is $e^-_L e^+_R$.

MI, $\mu^+\mu^-$**X,** $e^-_R e^+_L$					
N_{evts} Remained	$\mu^+\mu^-X$	$\mu^+\mu^-$	$\tau^+\tau^-$	$\mu^+\mu^-\nu\nu$	$\mu^+\mu^-ff$
Before any restriction	1967 (100.0%)	2.0M	1.2M	9k	291k
+ Lepton ID + Tightened Pre-Cuts	1667 (84.73%)	6696	3471	1048	5324
+ $P_{Tdl} > 20$GeV	1623 (82.48%)	5419	3037	957	4600
+ $M_{dl} \in (80, 100)$GeV	1544 (78.47%)	4347	2092	702	3530
+ $acop \in (0.2, 3.0)$	1448 (73.60%)	3592	113	656	3169
+ $\Delta P_{Tbal.} > 10$GeV	1421 (72.21%)	229	81	632	2873
+ $\lvert\Delta\theta_{2tk}\rvert > 0.01$	1419 (72.10%)	101	81	625	2851
+ $\lvert\cos\theta_{missing}\rvert < 0.99$	1379 (70.10%)	54	81	625	2065
+ $M_{recoil} \in (115, 150)$GeV	1367 (69.49%)	50	81	487	1506
+ $f_L > 0.19$	1165 (59.20%)	28	0	243	752

Table 7: Number of events left after each cut for the $\mu^+\mu^-X$ channel in the MI Analysis. Fractions of number of events remained of the Higgs-Strahlung process are given inside parentheses, the last one gives the efficiency of signal selection. The polarisation mode is $e^-_R e^+_L$.

MI, e^+e^-**X,** $e^-_R e^+_L$					
N_{evts} Remained	e^+e^-X	e^+e^-	$\tau^+\tau^-$	$e^+e^-\nu\nu$	e^+e^-ff
Before any restriction	2107 (100.0%)	4.3G	1.2M	17k	1.1M
+ Lepton ID + Tightened Pre-Cuts	1352 (64.16%)	40896	5257	1469	10198
+ $P_{Tdl} > 20$GeV	1313 (62.33%)	36742	4546	1351	8430
+ $M_{dl} \in (80, 100)$GeV	1177 (55.88%)	23993	3051	943	5909
+ $acop \in (0.2, 3.0)$	1103 (52.36%)	21846	107	881	5266
+ $\Delta P_{Tbal.} > 10$GeV	1077 (51.11%)	1612	92	805	4517
+ $\lvert\Delta\theta_{2tk}\rvert > 0.01$	1076 (51.05%)	927	92	799	4465
+ $\lvert\cos\theta_{missing}\rvert < 0.99$	1050 (49.82%)	638	92	799	3484
+ $M_{recoil} \in (115, 150)$GeV	1033 (49.04%)	539	12	586	2521
+ $f_L > 0.16$	909 (43.14%)	326	4	368	1294

Table 8: Number of events left after each cut for the e^+e^-X channel in the MI Analysis. Fractions of number of events remained of the Higgs-Strahlung process are given inside parentheses, the last one gives the efficiency of signal selection. The polarisation mode is $e^-_R e^+_L$.

MD, $\mu^+\mu^-$**X,** $e^-_L e^+_R$					
N_{evts} Remained	$\mu^+\mu^-X$	$\mu^+\mu^-$	$\tau^+\tau^-$	$\mu^+\mu^-\nu\nu$	$\mu^+\mu^-ff$
Before any restriction	2918 (100.0%)	2.6M	1.6M	111k	317k
+ Lepton ID + Tightened Pre-Cuts	2472 (84.72%)	9742	4582	9268	8175
+ $N_{add.TK} > 1$	2453 (84.05%)	604	842	145	6321
+ $\lvert\Delta\theta_{2tk}\rvert > 0.01$	2449 (83.91%)	63	816	14	6254
+ $\lvert\Delta\theta_{min}\rvert > 0.01$	2417 (82.81%)	38	261	1	5711
+ $acop \in (0.2, 3.0)$	2256 (77.29%)	32	0	1	5051
+ $\lvert\cos\theta_{missing}\rvert < 0.99$	2189 (75.00%)	16	0	1	3843
+ $M_{recoil} \in (115, 150)$GeV	2154 (73.81%)	15	0	1	2830
+ $f_L > 0.17$	1911 (65.49%)	11	0	0	1387

Table 9: Number of events left after each cut for the $\mu^+\mu^-X$ channel in the MD Analysis. Fractions of number of events remained of the Higgs-Strahlung process are given inside parentheses, the last one gives the efficiency of signal selection. The polarisation mode is $e^-_L e^+_R$.

MD, e^+e^-**X,** $e^-_L e^+_R$					
N_{evts} Remained	e^+e^-X	e^+e^-	$\tau^+\tau^-$	$e^+e^-\nu\nu$	e^+e^-ff
Before any restriction	3138 (100.0%)	4.3G	1.6M	147k	110k
+ Lepton ID + Tightened Pre-Cuts	2019 (64.33%)	43607	6422	13196	12548
+ $N_{add.TK} > 1$	2004 (63.87%)	3136	1740	374	10202
+ $\|\Delta\theta_{2tk}\| > 0.01$	2001 (63.77%)	655	1073	79	10095
+ $\|\Delta\theta_{min}\| > 0.01$	1969 (62.75%)	155	128	6	9271
+ $acop \in (0.2, 3.0)$	1840 (58.62%)	134	0	6	8366
+ $\|\cos\theta_{missing}\| < 0.99$	1792 (57.11%)	91	0	6	6696
+ $M_{recoil} \in (115, 150)$GeV	1731 (55.16%)	73	0	1	4950
+ $f_L > 0.27$	1378 (43.90%)	27	0	0	1652

Table 10: Number of events left after each cut for the e^+e^-X channel in the MD Analysis. Fractions of number of events remained of the Higgs-Strahlung process are given inside parentheses, the last one gives the efficiency of signal selection. The polarisation mode is $e^-_L e^+_R$.

MD, $\mu^+\mu^-$**X,** $e^-_R e^+_L$					
N_{evts} Remained	$\mu^+\mu^-X$	$\mu^+\mu^-$	$\tau^+\tau^-$	$\mu^+\mu^-\nu\nu$	$\mu^+\mu^-ff$
Before any restriction	1967 (100.0%)	2.0M	1.2M	9k	291k
+ Lepton ID + Tightened Pre-Cuts	1667 (84.73%)	6696	3471	1048	5324
+ $N_{add.TK} > 1$	1654 (84.07%)	415	391	9	4160
+ $\|\Delta\theta_{2tk}\| > 0.01$	1651 (83.93%)	41	379	0	4108
+ $\|\Delta\theta_{min}\| > 0.01$	1629 (82.81%)	22	105	0	3739
+ $acop \in (0.2, 3.0)$	1522 (77.34%)	20	0	0	3312
+ $\|\cos\theta_{missing}\| < 0.99$	1476 (75.03%)	11	0	0	2438
+ $M_{recoil} \in (115, 150)$GeV	1453 (73.85%)	10	0	0	1803
+ $f_L > 0.17$	1289 (65.53%)	8	0	0	875

Table 11: Number of events left after each cut for the $\mu^+\mu^-X$ channel in the MD Analysis. Fractions of number of events remained of the Higgs-Strahlung process are given inside parentheses, the last one gives the efficiency of signal selection. The polarisation mode is $e^-_R e^+_L$.

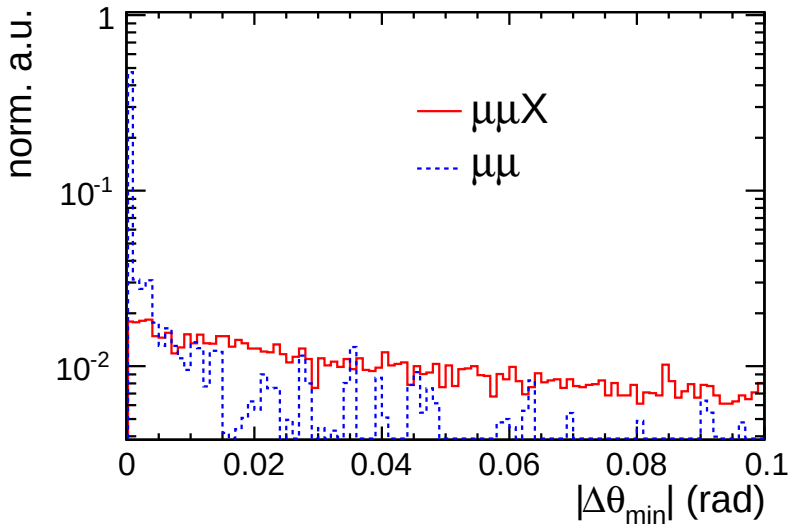

Figure 21: Distribution of $\Delta\theta$ between muon candidates and additional tracks, for the signal events ($\mu\mu X$) and background by muon pair creation ($\mu\mu$).

MD, e^+e^-**X**, $e^-_R e^+_L$					
N_{evts} Remained	e^+e^-X	e^+e^-	$\tau^+\tau^-$	$e^+e^-\nu\nu$	e^+e^-ff
Before any restriction	2107 (100.0%)	4.3G	1.2M	17k	1.1M
+ Lepton ID + Tightened Pre-Cuts	1352 (64.16%)	40896	5257	1469	10198
+ $N_{add.TK} > 1$	1342 (63.69%)	2935	1500	22	8227
+ $\|\Delta\theta_{2tk}\| > 0.01$	1340 (63.60%)	617	859	4	8133
+ $\|\Delta\theta_{min}\| > 0.01$	1319 (62.59%)	146	57	0	7388
+ $acop \in (0.2, 3.0)$	1232 (58.47%)	125	0	0	6651
+ $\|\cos\theta_{missing}\| < 0.99$	1201 (57.00%)	84	0	0	5265
+ $M_{recoil} \in (115, 150)$GeV	1161 (55.10%)	67	0	0	3886
+ $f_L > 0.32$	889 (42.20%)	20	0	0	1119

Table 12: Number of events left after each cut for the e^+e^-X channel in the MI Analysis. Fractions of number of events remained of the Higgs-Strahlung process are given inside parentheses, the last one gives the efficiency of signal selection. The polarisation mode is $e^-_R e^+_L$.

6 Extraction of Higgs Mass and the Higgs production Cross Section

In the previous section the criteria to select the signal events and to suppress the background from various sources have been introduced and applied. The remaining spectra are a superposition of signal and background events convoluted with beam effects. In the following, the relevant observables as the Higgs boson mass M_H and the total Higgs-strahlung cross section σ are extracted. Note in passing, that the results for the eeX-channel will always contain a small admixture of the ZZ fusion process.

As indicated above, the resulting spectrum is composed by several components. This motivates to approximate this spectrum in a non-parametric way using a Kernel Estimation as introduced in [14] and applied in [15, 16]. In order to reduce the effort of finding a parent function using either the already simulated data set or by simulating another independent set of data a so-called *Simplified Kernel Estimation* is proposed.

The signal spectrum is approximated by the following function:

$$F_S(x) = \frac{1}{N}\sum_{j=1}^{m} n_j G(x; t_j; h_j) \tag{2}$$

with

$$h_j = \left(\frac{4}{3}\right)^{1/5} N^{-1/5} \Delta x \sqrt{\frac{N}{n_j}}, \tag{3}$$

Here G is a Gaussian with the parameters $\mu = t_j$ where t_j is the center of the jth bin of a histogram with m bins and $\sigma = h_j$ where h_j is the *smoothing parameter* of bandwidth of the individual Gaussians placed around the bin centers. The parameter Δx is assumed to the the standard deviation in each bin and $\frac{n_j}{\Delta x N}$ is an estimate for the parent distribution. By the transformation $x \rightarrow x' = x - m_H$, the approximated function becomes sensitive to the value of the Higgs-Mass.

The background is approximated by a second order Chebyshev polynomial. By this statistical fluctuations in the remaining background events are smoothened. Using this polynomial as input the background is generated again with 40 times higher statistics. Therefore, statistical uncertainties are nearly excluded. The combination of signal and background is finally fitted by the sum of the signal and the background functions.

The simulated signal sample is separated into two sets of data. One of them, the *Reference Sample*, is employed to determine all fit parameters except the normalisation N of the signal signal and the actual Higgs mass, M_H. The normalisation N and the Higgs mass M_H enter as free parameters of the fit to the second sample, the *Result Sample*. The spectra of the Result Sample, scaled to a luminosity of $\mathcal{L}$=250 fb^{-1}, including the defined fitting function are displayed in Figures 24 and 25 for the Model Independent Analysis and in Figures 26 to 27 for the Model Dependent Analysis. The fit based on the Kernel estimation for the signal part describes the shape of the mass spectra very well and are therefore suited for the extraction of the relevant parameters which are listed in Table 13 for the Model Independent Analysis and in Table 14 for the Model Dependent Analysis. In [13] alternative fit methods are discussed which lead to nearly identical results.

Pol.	Ch.	M_H (GeV)	σ (fb)
$e^-_R e^+_L$ $\mathcal{L} = 250$ fb^{-1}	$\mu^+\mu^- X$	120.006 ±(0.039)	7.89 ± 0.28 (3.55 %)
	$e^+e^- X$	120.005 ±(0.092)	8.46 ± 0.43 (5.08 %)
	merged	120.006 ±(0.036)	8.06 ± 0.23 (2.91 %)
$e^-_L e^+_R$ $\mathcal{L} = 250$ fb^{-1}	$\mu^+\mu^- X$	120.008 ±(0.037)	11.70 ± 0.39 (3.33 %)
	$e^+e^- X$	119.998 ±(0.085)	12.61 ± 0.62 (4.92 %)
	merged	120.006 ±(0.034)	11.96 ± 0.33 (2.76 %)

Table 13: Resulting Higgs mass M_H and cross section σ of the *MI Analysis* using *Kernel Estimation*.

Pol.	Ch.	M_H (GeV)	σ (fb)
$e^-_R e^+_L$ $\mathcal{L} = 250$ fb^{-1}	$\mu^+\mu^- X$	120.008 ± 0.037	7.88 ± 0.26 (3.30 %)
	$e^+e^- X$	120.001 ± 0.081	8.46 ± 0.38 (4.49 %)
	merged	120.007 ± 0.034	8.06 ± 0.21 (2.66 %)
$e^-_L e^+_R$ $\mathcal{L} = 250$ fb^{-1}	$\mu^+\mu^- X$	120.009 ± 0.031	11.68 ± 0.32 (2.74 %)
	$e^+e^- X$	120.007 ± 0.065	12.58 ± 0.46 (3.66 %)
	merged	120.009 ± 0.028	11.97 ± 0.26 (2.19 %)

Table 14: Resulting Higgs mass M_H and cross section σ of the *MD Analysis* using *Kernel Estimation*.

6.1 Discussion of the Results

The Higgs mass can be determined to a precision of the order of 0.03% when the eeX channel and the $\mu\mu X$ are combined. Regarding the individual results, it can be deferred that the precision in the $\mu\mu X$ channel is more than two times smaller than that of the eeX Channel This increase of the error is mainly induced by bremsstrahlung of the electrons in the detector material. This can be concluded by comparing the results between Tables 13 and 14 as for the latter the background of Bhabha scattering is suppressed while the difference in the precision between the two decay modes of the Z bosons remains the same. The precision on the cross section is less sensitive to this experimental drawback as it is derived within a basically arbitrary mass window. The derived values for the Model Dependent Analysis are consistently slightly more precise. The relatively small difference of the results confirms that the methods employed for background suppression in the Model Independant Analysis are already very efficient.

	$\Delta M_{tot.}$ (MeV)	$\Delta M_{mac.}$ (MeV)	$\Delta M_{dec.}$ (MeV)
$\mu\mu X$	650	560	330
eeX	750	560	500

Table 15: Mass Resolution with contributions by machine ($\Delta M_{mac.}$) and detector ($\Delta M_{det.}$) separated.

The width of the Higgs boson mass as shown before is mainly given by a convolution of detector uncertainties and uncertainties on the energy of the incoming beams. Uncertainties on the energy of the incoming beams are imposed by accelerator components such as the initial linac, the damping rings or, in the case of electrons, by a tentative undulator in the electron beam line. Another source of uncertainty is the beamstrahlung when particles of a

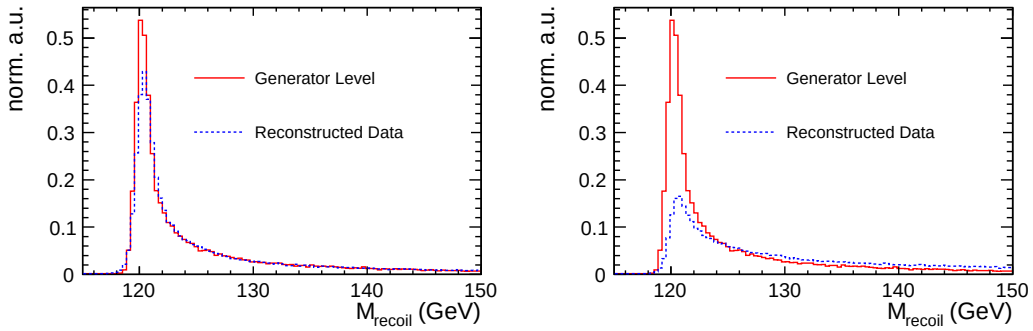

Figure 22: Comparisons of recoil mass spectra in generator level and after full simulation, for the $\mu\mu X$-channel (left) and the eeX-channel (right).

beam bunch interact in the electromagnetic field of the opposite one. The Figure 22 shows the Higgs mass spectrum before and after full detector simulation. The detector response leads only to small additional widening of the maximum of the recoil mass distribution. Using a Gaussian fit to the left side of the recoil mass distribution, the width before detector simulation can be quantified to be 560 MeV while it increases to 650 MeV for the $\mu\mu X$ channel after detector simulation, see Table 15. For the given configuration, the uncertainty on the incoming beams remains the dominant contribution to the observed width even for the eeX channel.

On the Control of Systematic Errors

Naturally, the measurement of the Higgs mass is sensitive to the calibration of the detector and the beam energies as the Higgs mass is directly computed from the four momenta of the particles composing the di-lepton system and the centre-of-mass energy. Both uncertainties can be controlled by the measurement of the $e^+e^- \rightarrow ZZ$ process as the Z mass is known to a few MeV and the cross section for Z pair production is approximately 40 times higher than that of the Higgs-strahlungs process. Once the detector is calibrated the Higgs-strahlung process can be used to determine, within reasonable limits, arbitrary Higgs masses. The algorithms presented in this note are also suited for the quantification of the systematic error. Note, that the systematic error of the cross section determination might be easier to control by using a smaller set of cut variables than those presented above. Such a set could comprise only the invariant mass and the transverse momentum of the di-lepton system, M_{dl}, P_{Tdl} or, in case of the model dependant analysis, the number of additional tracks, $N_{add,TK}$. The expected increase of the statistical error is only about 10%.

6.1.1 Recovery of Bremsstrahlungs Photons

The lower precision obtained in the eeX-Channel is due to the Bremsstrahlung of the final state electrons in the passive material of the detector. In the following an attempt is made to improve the precision in that channel by recovering the bremsstrahlungs photons [17]. The four momenta of the selected electrons are combined with those of photons which have a small angular distance to the electrons. If these combined objects together with the corresponding other electron candidate form the Z mass, they are included in the Z reconstruction. The inclusion of low energetic photons leads to a penalty in the momentum reconstruction due to

the poor energy resolution of the electromagnetic calorimeter for low energetic particles. This drawback might get counterbalanced by the gain in statistics due to the described recovery of the energy loss.

Figure 23 shows the recoil mass spectrum after the recovery of the Bremsstrahlungs photons. The worse resolution around the mass maximum is clearly visible. The corresponding results are given Tables 16 through 17 and the fitted spectra in Figures 28 through 29. The numbers show that the mass resolution is improved by 10% while the precision in the cross section is improved by 20%. The cross section benefits directly from the gain in statistics while the determination of the recoil mass suffers from the reduced momentum resolution.

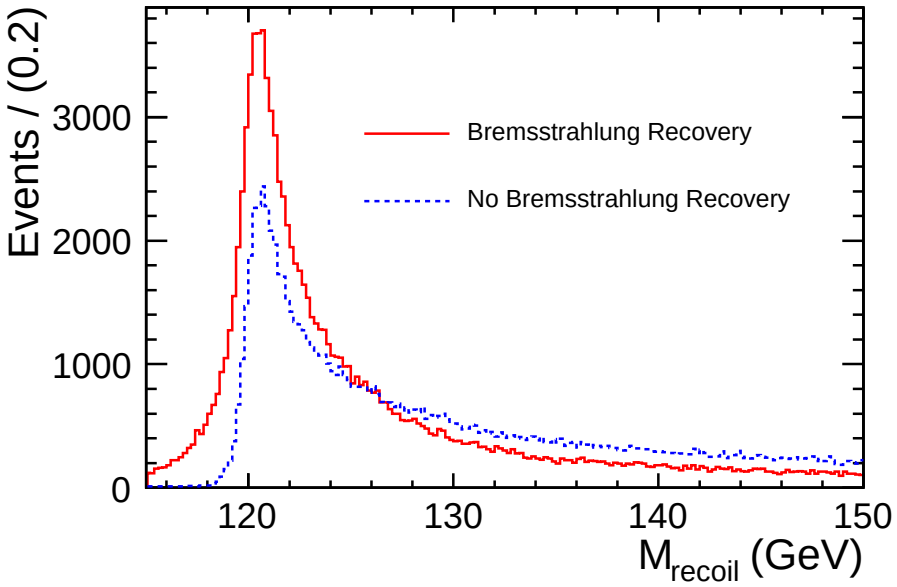

Figure 23: Comparison of the Higgs recoil mass distributions of e^+e^-X channel with and without the bremsstrahlung photons recovery.

Ana.	Pol.	Ch.	S (%)	B
MI	$e^-_R e^+_L$	e^+e^-X	1029 (48.84%)	1408
	$e^-_L e^+_R$	e^+e^-X	1491 (41.51%)	3394
MD	$e^-_R e^+_L$	e^+e^-X	1152 (54.66%)	1114
	$e^-_L e^+_R$	e^+e^-X	1724 (54.94%)	1513

Table 16: Resulting Number of Signal (S) and Number of Background (B), and the efficiencies of signal selection (in the parentheses) after background rejection, for eeX channel with *Bremsstrahlung Photons Recovery*

7 Conclusion and Outlook

Using mainly the Higgs-strahlung process with the Z boson decaying leptonically and a Higgs boson mass of 120 GeV as input, the current design of the ILD detector promises to determine the mass of the Higgs boson to a precision of the order of 30 MeV. According to [18]

Ana.	Pol.	M_H (GeV)	σ (fb)
MI	$e^-_R e^+_L$	120.003 ± 0.081	8.41 ± 0.36 (4.28 %)
	$e^-_L e^+_R$	119.997 ± 0.073	12.52 ± 0.49 (3.91 %)
MD	$e^-_R e^+_L$	119.999 ± 0.074	8.41 ± 0.31 (3.69 %)
	$e^-_L e^+_R$	120.001 ± 0.060	12.51 ± 0.38 (3.04 %)

Table 17: Resulting Higgs mass M_H and cross section σ for the *Model Independent Analysis* and *Model Dependent Analysis* of the Higgs-Strahlung pr ocess of e^+e^-X channel with *Bremsstrahlung photons Recovery*.

and references therein, such a precision renders sensitivity to effects from super-symmetric extensions to the Standard Model. Assuming a heavier Higgs, the precision might allow also for the determination of the Higgs boson mass width at centre-of-mass energies higher than 250 GeV. Staying with small Higgs masses, it has been demonstrated semi-analytically [18] and confirmed with full simulation studies [19] that the precision can be further increased by working at a centre-of-mass energy close to the HZ production threshold, i.e. at $\sqrt{s}$=230 GeV. In the present study, the cross section and therefore the coupling strength at the HZZ vertex is determined to a precision of the order of 2-3% which might already be sufficient to get sensitive to contributions to this coupling from physics beyond the Standard Model.

The signal to background ratio can be enhanced to a value of at least 30% even if the cross sections of the background processes are several orders of magnitudes higher. The background suppression exploits the considerable capabilities of track recognition as allowed by the current design of the ILD detector. The precision of the measurement can be improved by a better muon recognition by e.g. including a muon system in the analysis which has not been done so far. The precision obtained in the branch in which the Z boson decays into electrons might gain considerably from a revision of the amount of passive material in the detector. Both decay modes may gain also from an exploitation of the particle identification of the ILD detector by means of a dE/dx measurement in the TPC. For this, further studies are needed. A future study clearly will have to quantify the systematic uncertainties and to identify those which have the largest influence on the systematic errors. This would give important directions on the final detector layout and the precision needed for e.g. alignment systems. For such a study realistic inputs on e.g. the uncertainty of drift times in the TPC or residual misalignments after detector movements are needed.

The analysis has proven that the results are sensitive to details of the accelerator configuration. Using the set of parameters as has been chosen for the SLAC samples which in turn correspond to the current best knowledge of the beam parameters, approximately half of the statistical error is generated by uncertainties caused by beamstrahlung and the energy spread of the incoming beams. The Higgs-strahlung process constitutes an important benchmark for the optimisation of the accelerator performance.

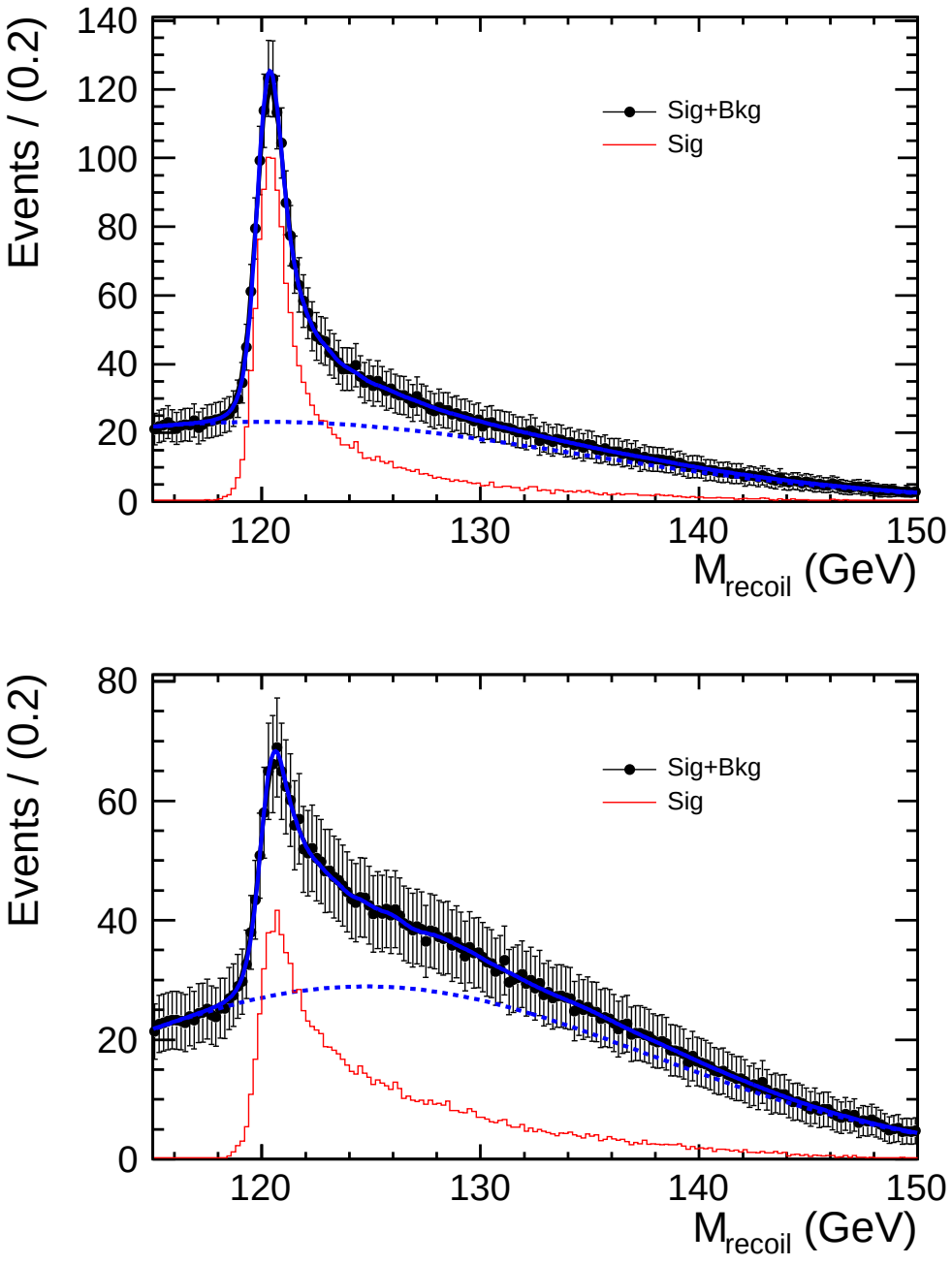

Figure 24: Reconstructed Higgs mass spectrum together with the sum of underlying background for the *Model Independent Analysis* for the $\mu\mu X$-channel (top) and eeX-channel (bottom). The polarisation mode is $e^-_L e^+_R$. The lines show the fits using the Simplified Kernel Estimation fitting formula to the signal and a polynomial of second order to the background as explained in the text.

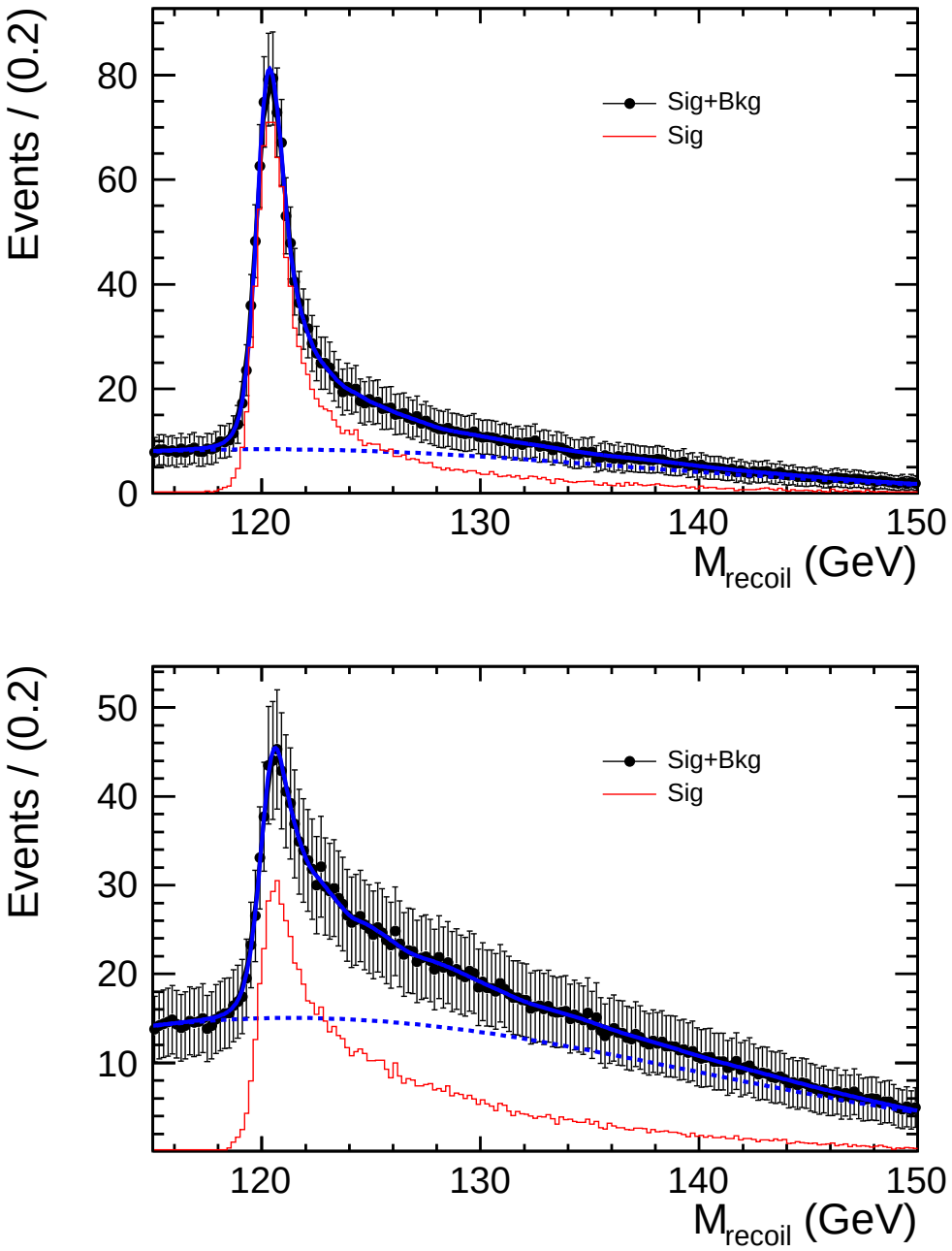

Figure 25: Reconstructed Higgs mass spectrum together with the sum of underlying background for the *Model Independent Analysis* for the $\mu\mu X$-channel (top) and eeX-channel (bottom). The polarisation mode is $e^-_R e^+_L$. The lines show the fits using the Simplified Kernel Estimation fitting formula to the signal and a polynomial of second order to the background as explained in the text.

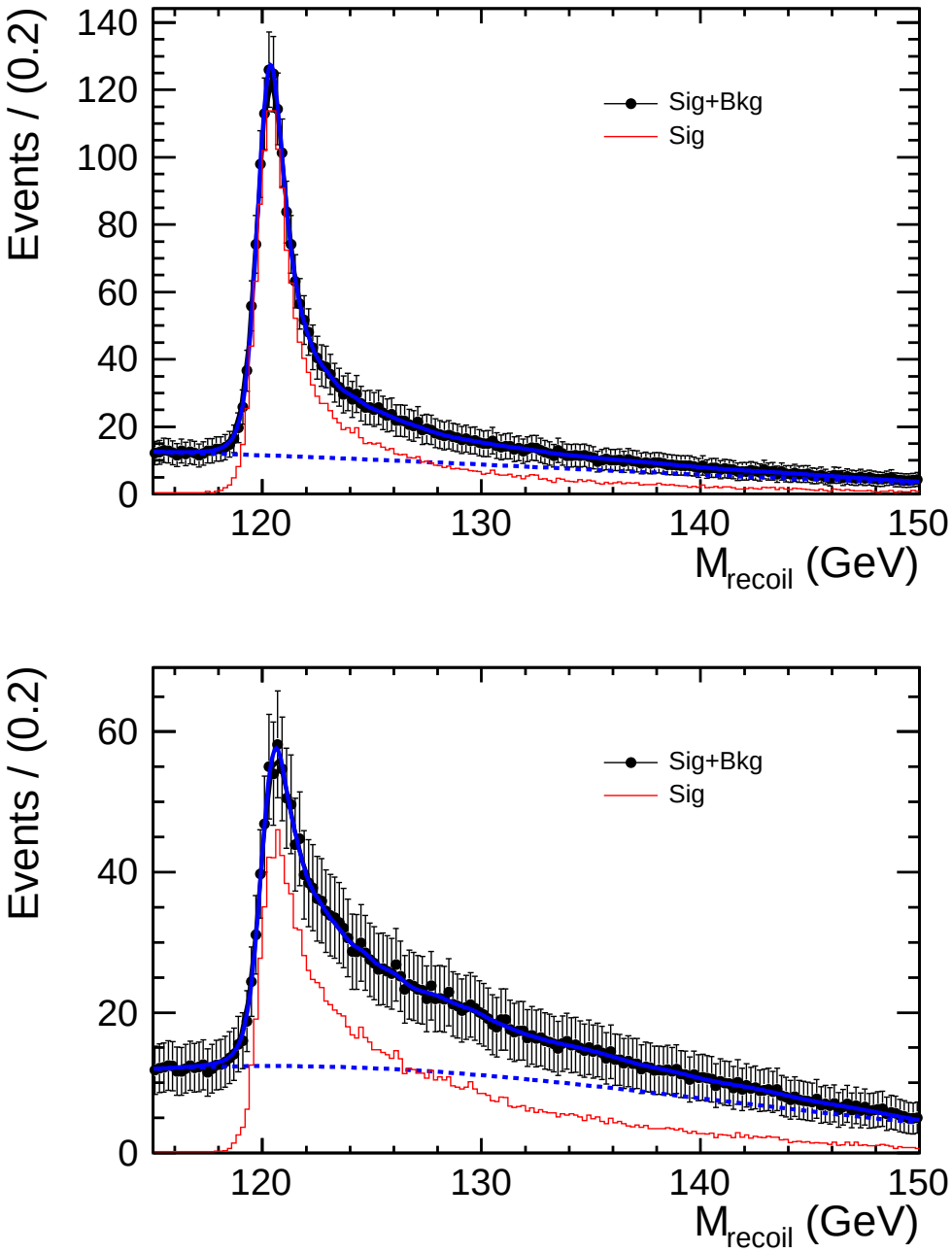

Figure 26: Reconstructed Higgs mass spectrum together with the sum of underlying background for the *Model Dependent Analysis* for the $\mu\mu X$-channel (top) and eeX-channel (bottom). The polarisation mode is $e^-_L e^+_R$. The lines show the fits using the Simplified Kernel Estimation fitting formula to the signal and a polynomial of second order to the background as explained in the text.

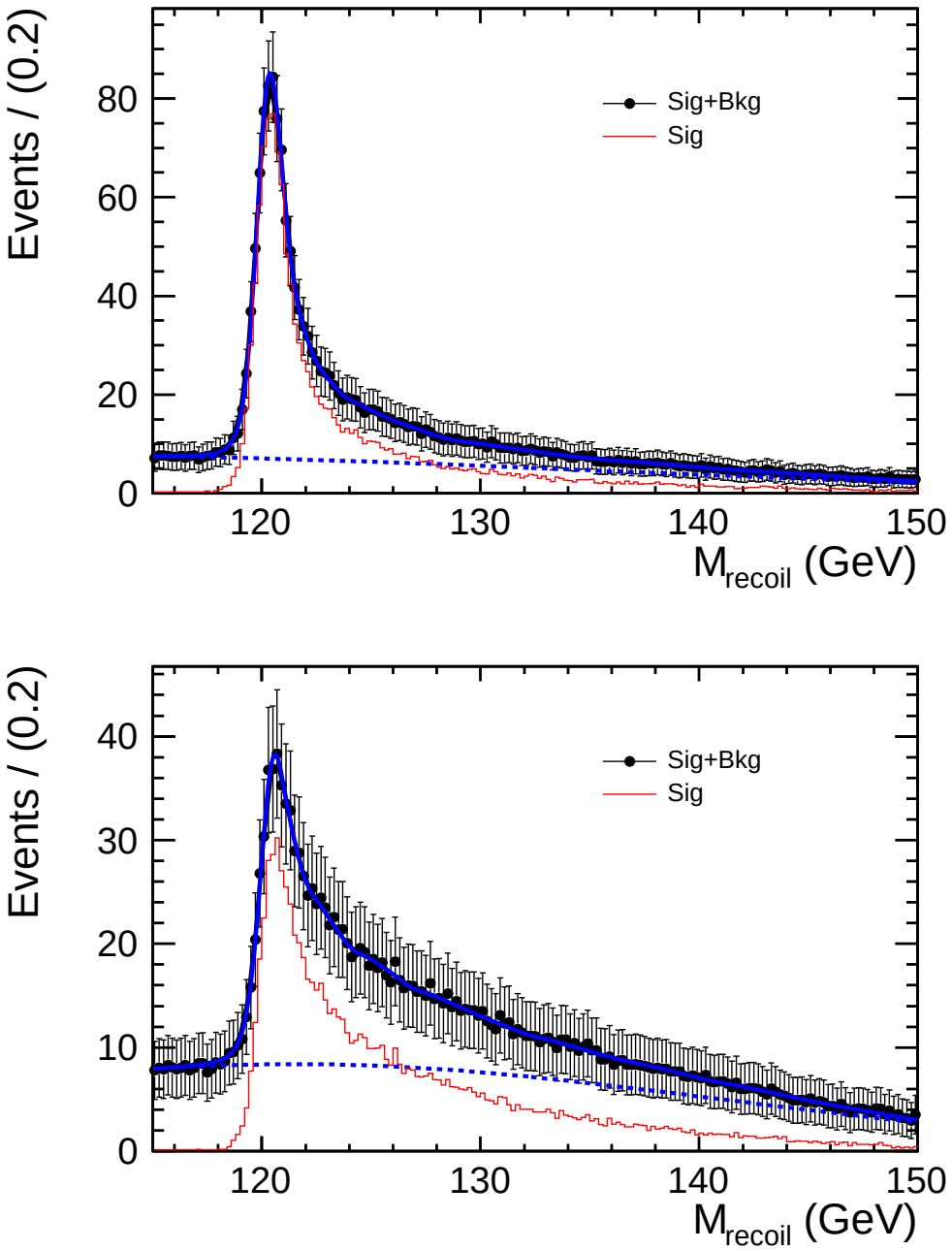

Figure 27: Reconstructed Higgs mass spectrum together with the sum of underlying background for the *Model Dependent Analysis* for the $\mu\mu X$-channel (top) and eeX-channel (bottom). The polarisation mode is $e^-_R e^+_L$. The lines show the fits using the Simplified Kernel Estimation fitting formula to the signal and a polynomial of second order to the background as explained in the text.

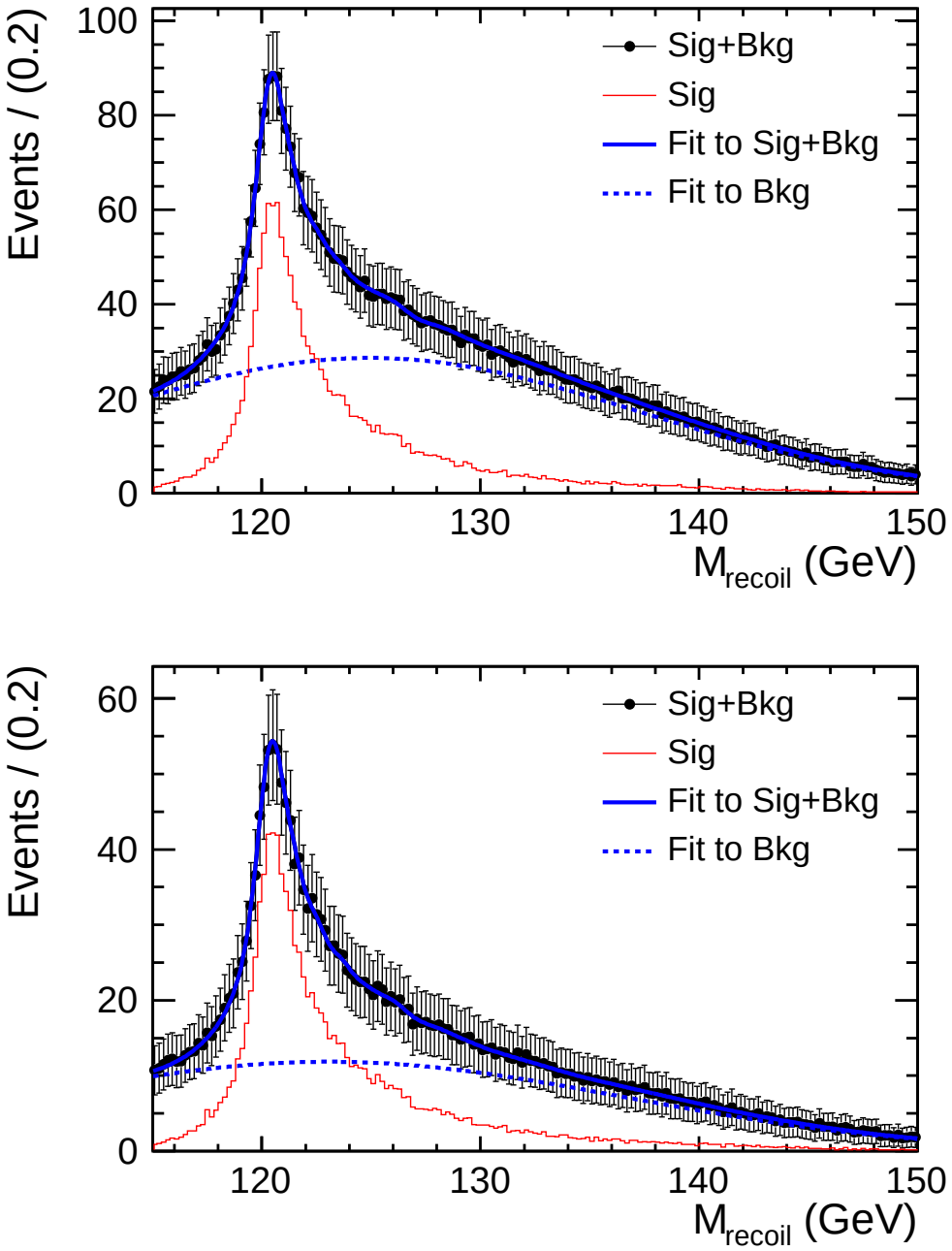

Figure 28: Reconstructed Higgs mass spectrum *after the recovery of Bremsstrahlungs photons* together with the sum of underlying background for the *Model Independent Analysis* for eeX-channel. The polarisation mode is $e^-_L e^+_R$ (top) and $e^-_R e^+_L$ (bottom). The lines show the fits using the Simplified Kernel Estimation fitting formula to the signal and a polynomial of second order to the background as explained in the text.

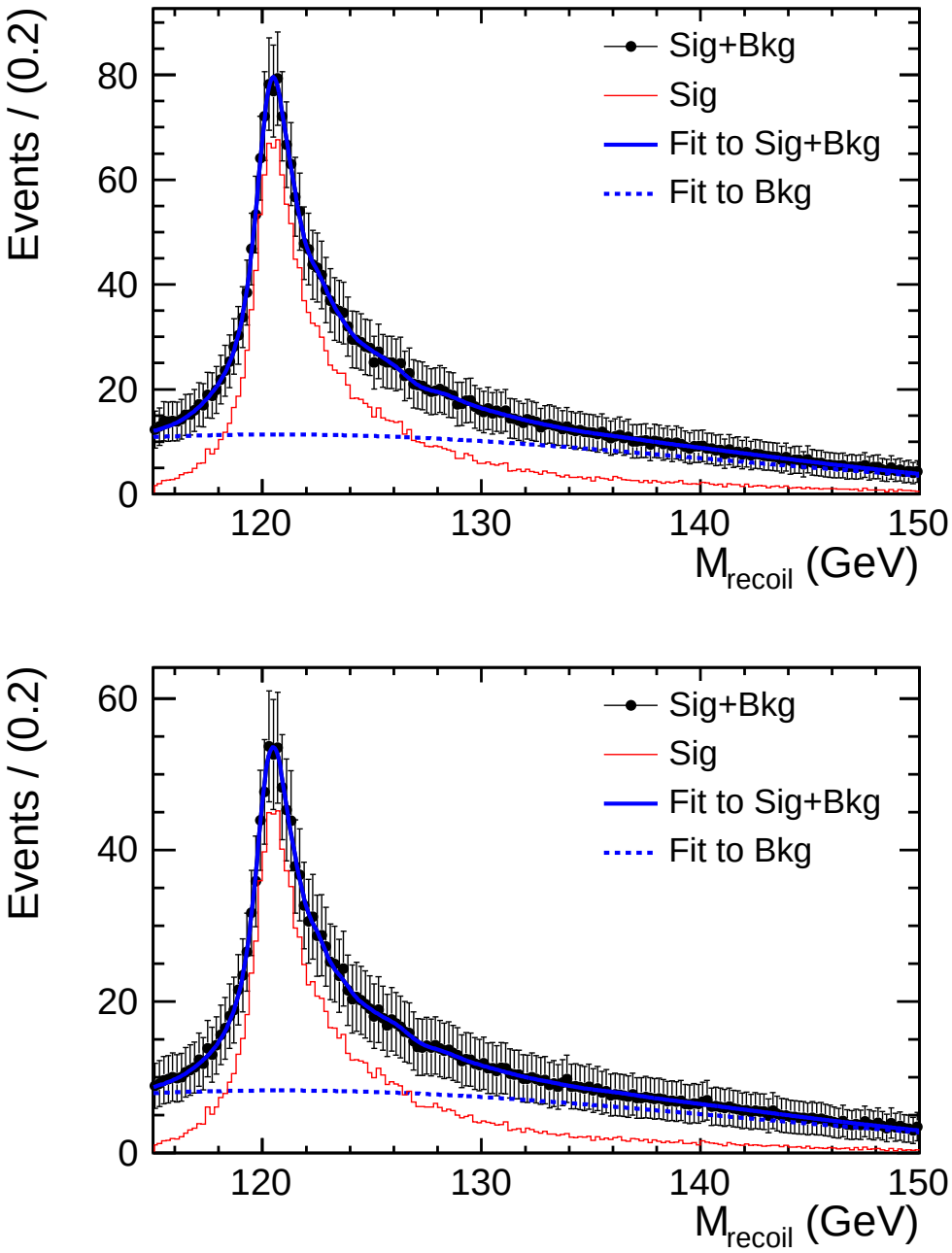

Figure 29: Reconstructed Higgs mass spectrum *after the recovery of Bremsstrahlungs photons* together with the sum of underlying background for the *Model Dependent Analysis* for eeX-channel. The polarisation mode is $e^-_L e^+_R$ (top) and $e^-_R e^+_L$ (bottom). The lines show the fits using the Simplified Kernel Estimation fitting formula to the signal and a polynomial of second order to the background as explained in the text.

References

[1] The LEP Electroweak Working Group, arXiv:0811.4682 [hep-ex] (November 2008) and updates for 2009 summer conferences, see `http://lepewwg.web.cern.ch/LEPEWWG/plots/summer2009/`.

[2] The Higgs Working Group at Snowmass '05, arXiv:hep-ph/0511332 (November 2005).

[3] W. Lohmann *et al. Prospects to Measure the Higgs Boson Mass and Cross Section in ee* $\rightarrow$ ZH *Using the Recoil Mass Spectrum*, arXiv:0710.2602v1 [hep-ex] (October 2007).

[4] M. Ruan *et al.*, *A precision determination of Higgs mass using the fully simulated Higgs-strahlung process* $e^+e^- \rightarrow hZ \rightarrow h\mu\mu$ *at ILC*, CARE-Note-2008-0013-ELAN

[5] M. Battaglia *et al.*, arXiv:hep-ex/0603010v1 (March 2006).

[6] The ILD Group, *ILD - Letter of Intent*, `http://www.ilcild.org/documents/ild-letter-of-intent` (2009).

[7] W. Kilian, T. Ohl, J. Reuter, *WHIZARD: Simulating Multi-Particle Processes at LHC and ILC* , arXiv:0708.4233 [hep-ph] (August 2007).

[8] D. Schulte, *GUINEA-PIG - An* e^+e^- *beam simulation program*, PhD Thesis University of Hamburg (1996).

[9] M. Berggren, Talk in ILD Optimisation Meeting 13/5/09, `http://ilcagenda.linearcollider.org/conferenceDisplay.py?confId=3585`.

[10] `http://ilcsoft.desy.de`.

[11] The GEANT4 collaboration, NIM **A** 506 (2003) 250-303.

[12] J.C. Brient, *Measurement of the Higgs Mass and* e^+e^- $\rightarrow$ ZH *cross sections at Linear Colliders*, LC-PHSM-2000-049.

[13] H. Li, PhD Thesis Université Paris Sud XI and LAL Orsay, LAL 09-118.

[14] K. S. Cranmer, *Kernel estimation in High-energy physics*, Comput. Phys. Commun. **136** (2001) 198, hep-ph/0005309.

[15] K. S. Cranmer, *Kernel Estimation for Parametrization of Discriminant Variable Distributions*, ALEPH 99-144, PHYSIC 99-05 (1999).

[16] The OPAL Collaboration, *Search for Neutral Higgs Bosons in* e^+e^- *Collisions at* $\sqrt{s} \approx$ *192–202 GeV*, OPAL PHYSICS NOTE PN426 (2000).

[17] M. Thomson, *Private Communication, MARLIN Processor.*

[18] P. Bambade and F. Richard *Strategies to measure the Higgs mass, width and invisible decays at ILC*, arXiv:hep-ph/0703173 (March 2007).

[19] H. Li *et al. Precision Measurements of SM Higgs Recoil Mass and Cross Section for Ecm of 230 GeV and 250 GeV at ILC*, arXiv:0901.4893v3 [hep-ex] (January 2009).